

Electronic Supporting Information

The Effect of THF and the Chelating Modifier DTHFP on the Copolymerisation of β -Myrcene and Styrene: Kinetics, Microstructures, Morphologies, and Mechanical Properties

Dominik A. H. Fuchs,^a Hanna Hübner,^b Tobias Kraus,^c Bart-Jan Niebuur,^c Markus Gallei,^b Holger Frey,^{*a} Axel H. E. Müller^{*a}

^aDepartment of Chemistry, Johannes Gutenberg University, Duesbergweg 10-14, 55128 Mainz, Germany. *hfrey@uni-mainz.de, *axel.mueller@uni-mainz.de

^bChair in Polymer Chemistry, Saarland University, 66123 Saarbrücken, Germany

^cINM-Leibniz-Institute for New Materials, Campus D2 2, Saarland University, 66123 Saarbrücken, Germany and Colloid and Interface Chemistry, Saarland University, 66123 Saarbrücken, Germany

Table of Contents

1	Materials and Experimental Procedures	2
2	Instrumentation	3
3	Molecular weight determination	6
4	Copolymerisation Kinetics and Determination of Reactivity Ratios	7
5	Kinetics of Homopolymerisation of Myrcene	19
6	Copolymer composition	22
7	Microstructure of the Myrcene Units.....	24
8	Thermal properties.....	38
9	Copolymer Morphologies	40
10	Mechanical properties.....	42
	References.....	46

1 Materials and Experimental Procedures

1.1 Purification of Materials

All reactions were carried out under Schlenk conditions. Through a pressure valve a constant overpressure of 50 mbar between the argon gas cylinder and the Schlenk line was maintained at any time. All glassware used was tested under vacuum (10^{-3} mbar) and heated with a Bunsen burner for about 5 minutes and then cooled to room temperature. Subsequently, the glass vessel was filled with argon to create a dry inert gas atmosphere. This process was carried out a total of three times to ensure the absence of moisture and contaminants. The monomers β -myrcene and styrene were filtered through a column containing basic alumina to remove stabilizer. The monomers were dried over CaH_2 for one day at room temperature, degassed by three freeze thaw cycles and cryo-transferred into another flask containing $\text{Al}(\text{Oct})_3$, obtained by evaporation of hexane from a solution under reduced pressure for one day. To ensure complete cryo-transfer, the monomer volume was measured in a graduated ampoule and typically showed a loss of less than 1.5 %_{Vol} with respect to the combined volume of the monomers. This was explained by the loss of monomer during cryotransfer (autopolymerization and the high boiling point of β -myrcene), as well as volume contraction caused by miscibility.

Cyclohexane was dried under reflux with sodium and benzophenone under an argon atmosphere for at least 4 days. During this process the colour of the solution changed from colourless to dark blue, indicating complete absence of water. Subsequently the dry solvent was transferred into the reaction flask (Morton flask glass reactor), equipped with a NIR probe in an additional glass joint.t.

One litre of THF was dried with approximately 10 ml of *sec*-BuLi. To avoid reaction of THF with *sec*-BuLi, a small excess of 1,1-diphenylethylene (DPE) was added. Subsequently, it was cryo-transferred into a flask or ampoule. For small amounts of THF, a flask with a septum was used. A syringe was used to transfer the desired amount of THF to the reaction flask in argon countercurrent. DTHFP was dried in analogy to the monomers, and the dried compound was stored in the glovebox. For the small amounts of modifier, a dilution series with dry cyclohexane was prepared to simplify the addition.

1.2 Synthesis of copolymers with polar modifiers

The reaction set-up and synthesis is based on our earlier work.^{1,2}

All polymerizations were performed in the same manner, solely varying the amount of modifier employed.. As an example the synthesis of the polymer P(S-*co*-Myr) for $[\text{THF}]/[\text{Li}] = 80$ is described. After drying the reaction flask was filled with 600 ml (5.56 mol) of dry cyclohexane and 6.75 ml (0.083 mol, 80 eq) THF was added by syringe. The NIR baseline was recorded using Omnic software. Once the baseline was stable and the reaction solution reached a temperature of 20°C, polymerisation and kinetic measurements were started. The monomers styrene (55.3 ml, 0.48 mol) and myrcene (41.6 ml, 0.24 mol) were added via an ampoule, and the reaction was initiated by the addition of 0.8 ml (1.04 mmol, 1 eq) of a 1.3 molar solution of *sec*-BuLi in cyclohexane. This caused the solution to turn dark yellow. After 250 minutes, the kinetic measurement was stopped, the colour of the reaction solution had become less intense. The reaction was terminated by addition of 1.5 ml of degassed isopropanol under argon, and the reaction solution turned colourless again. The polymer was then precipitated from the reaction solution using 3.5 liters of a 1:3 mixture of isopropanol:methanol. The colourless polymer was dried under reduced pressure for at least one week, cut up and stored at -20°C.

Polymers with low dispersity between 1.06-1.10 and high yields between 86%-99% could be synthesized. It can be assumed that the polymerizations proceeded quantitatively. Slightly lower yields were obtained from polymerisations that did not form block structures and therefore could not be precipitated as fine powders. These samples possessed rather sticky nature, leading to a loss of more material during transfer to the storage vessels.

The dielectric constant LM of the solvent is calculated according to the following equation:³

$$\varepsilon_{LM} = \varepsilon_{CyH} + (\varepsilon_{modifier} - \varepsilon_{CyH}) * f_{modifier}$$

$f_{modifier}$ stands for the mole fraction of the modifier used. The dielectric constant for THF at 20°C is 7.58⁴ and for cyclohexane 2.023.⁵ No literature reference could be found for DTHFP. However, since DTHFP was added only in very small amounts, it can be assumed, according to the equation, that it is not noticeably different from pure cyclohexane.

2 Instrumentation

2.1 Reaction Monitoring via NIR Spectroscopy

Near-infrared spectra were obtained using a *Nicolet Magna 560 FT-IR* spectrometer and the *Omnic 7.4 Thermo Scientific* software. The detector is a PbS detector with a CaF₂ beam splitter, the light source is an IR laser with an aperture of 88, a mirror velocity of 0.6329, and an internal ADC gain of 8. The data interval in which the measurement took place was 1,928 cm⁻¹ with an internal resolution of 4. 8000-14000 spectra recorded in the range 5900-6250 cm⁻¹ with up to 7 scans per spectrum. The NIR probe head was connected by optical fibre. A background spectrum was generated before each experiment under the same conditions with at least 64 scans. All spectra were stored as individual spectra and evaluated using the *NIREVAL* software, as described in the *NIREVAL* user manual.

2.2 Temperature Monitoring

Temperature profiles were recorded at a time interval of 10 seconds by a LOG200-E temperature logger from Dostmann electronic GmbH. As an example, the temperature profile of the copolymerization in absence and presence of 2500 eq THF is given. Without modifier, the temperature fluctuation corresponds to the fluctuation in the lab. For 2500 eq THF a drastic temperature increase was detected during the first minutes of the reaction, which corresponds to the polymerization of styrene.

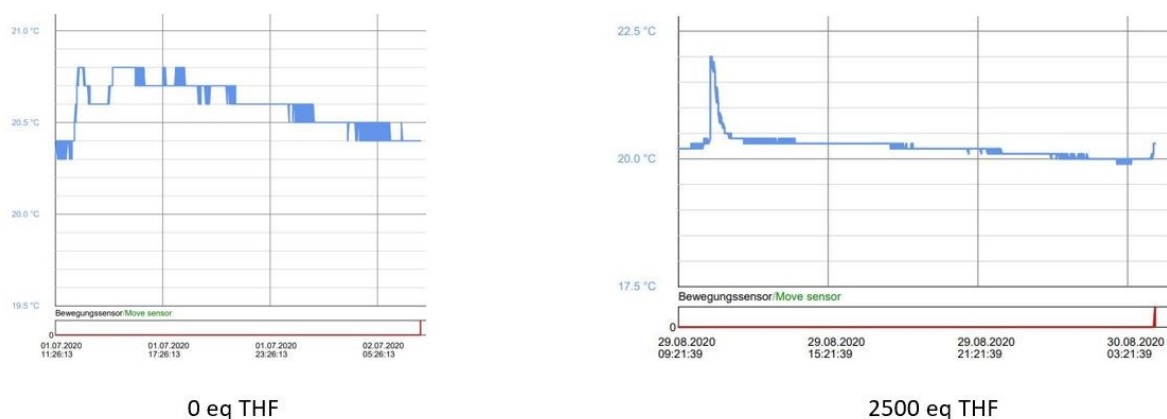


Figure S1: Temperature profile of the styrene myrcene copolymerisation in the presence of $[THF]/[Li] = 0$ and 2500.

2.3 NMR spectroscopy

NMR spectra were obtained using a Bruker Avance III 600 spectrometer at 600 MHz for ^1H -NMR and 151 MHz for ^{13}C -NMR spectra were measured. A 5 mm TCI cryo sample holder with z-gradient and ATM was used. Signals were referenced to the signal of the deuterated solvent. The chemical shift δ is given in parts per million (ppm).

The evaluation of the measured spectra was performed using MestReNova v13.1.0 from Mestrelab Research S. L. (Santiago de Compostela, Spain). For the measurement, approximately 100 mg of polymer was dissolved in 0.7 mL of CDCl_3 .

2.4 Gel Permeation Chromatography (GPC)

GPC was performed using the Agilent 1100 instrument from Waters 717 plus contained a MZ-Gel SD plus $10^5/10^3/100 \text{ \AA}$ columns from MZ-Analysetechnik (Mainz, Germany). The detector used was a RI detector (Agilent G1362A). The eluent was THF the injection volume was 100 μl . All measurements were performed at 20°C and a flow rate of 1.0 mL/min. Toluene served as internal standard and the molecular weight measurements were performed by calibration with polystyrene standard from PSS Polymer Standard Service GmbH (Mainz, Germany). The software WinGPC Unity of the company PSS (Mainz, Germany) has been used for the analysis of GPC data. For the measurement, approximately 1 mg of the polymer was dissolved in 2.5 ml THF and mixed with a drop of toluene added.

2.5 Differential scanning calorimetry

DSC measurements were performed using the Perkin Elmer DSC 8500 instrument. Calibration was performed with *n*-decane and an indium standard. The measurements were performed by a multi-point baseline correction and normalized to sample mass. Two heating and one cooling cycle were performed at a rate of 20 K/min in a temperature range of -80 to 130°C. The glass transition temperature was taken from the second heating cycle.

2.6 Transmission electron microscopy

TEM measurements were performed on a JEOL JEM-2100 electron microscope at 200kV; 0.14 nm resolution and a Gatan Orius SC1000 camera (binning 2; 1024x1024 pixels) in brightfield mode. The camera was computerized by the software Digital Micrograph Software controlled by Gatan. For the

measurement, polymer films were prepared by slow evaporation of the solvent CHCl_3 . These were treated at 120°C for 16 hours in an oven and then cut at -80°C into 50-70 nm thick slices. Subsequently, these slices were stained with OsO_4 to obtain the PMyr domains electron opaque.

2.7 Small-angle X-ray spectroscopy

Small-Angle X-ray Scattering (SAXS) experiments were carried out on a laboratory-scale Xeuss 2.0 instrument (Xenoxs, Grenoble, France). The X-ray beam of a copper K_α source with a wavelength of 0.154 \AA was focused on the sample with a spot size of 0.25 mm^2 . Measurements were performed at a sample-detector distance of 2520 mm, resulting in an accessible range of momentum transfers q of $0.05 - 0.23 \text{ \AA}^{-1}$. The momentum transfer q is defined as $q = 4\pi \cdot \sin(\theta/2)/\lambda$, with θ being the scattering angle that was calibrated using a standard silver behenate sample. The data were azimuthally integrated to obtain $I(q)$. The samples were placed directly in the beam, without the need of using a sample container. The acquisition time for each sample was 1h.

2.8 Tensile-elongation tests

Tensile-elongation tests were carried out on a Zwick/Roell Z005 machine. For this purpose, dog-bone structures of polymer films were punched out, which were formed by slow evaporation of the solvent CHCl_3 . The used specimens had a length of 22 mm and a width of 4 mm. To prepare the polymer films, approximately 3.8 g of polymer was dissolved in 30 ml of CHCl_3 and poured into a Petri dish with a diameter of 7 cm. This Petri dish was located horizontally in a desiccator filled with CHCl_3 . This desiccator was opened slightly to allow the solvent to slowly evaporate over a period of XXXapprox.. 3 weeks. Subsequently, the polymer films were stored for one week at a reduced pressure of 12 mbar. These films had a thickness of 0.3-0.7 mm. It was an initial force of 0.1 N applied to the specimen and then pulled at a speed of 10 mm/min. The dependence of the stress on the tensile was measured. Material properties were determined from 3-12 independent tensile experiments.

3 Molecular weight determination

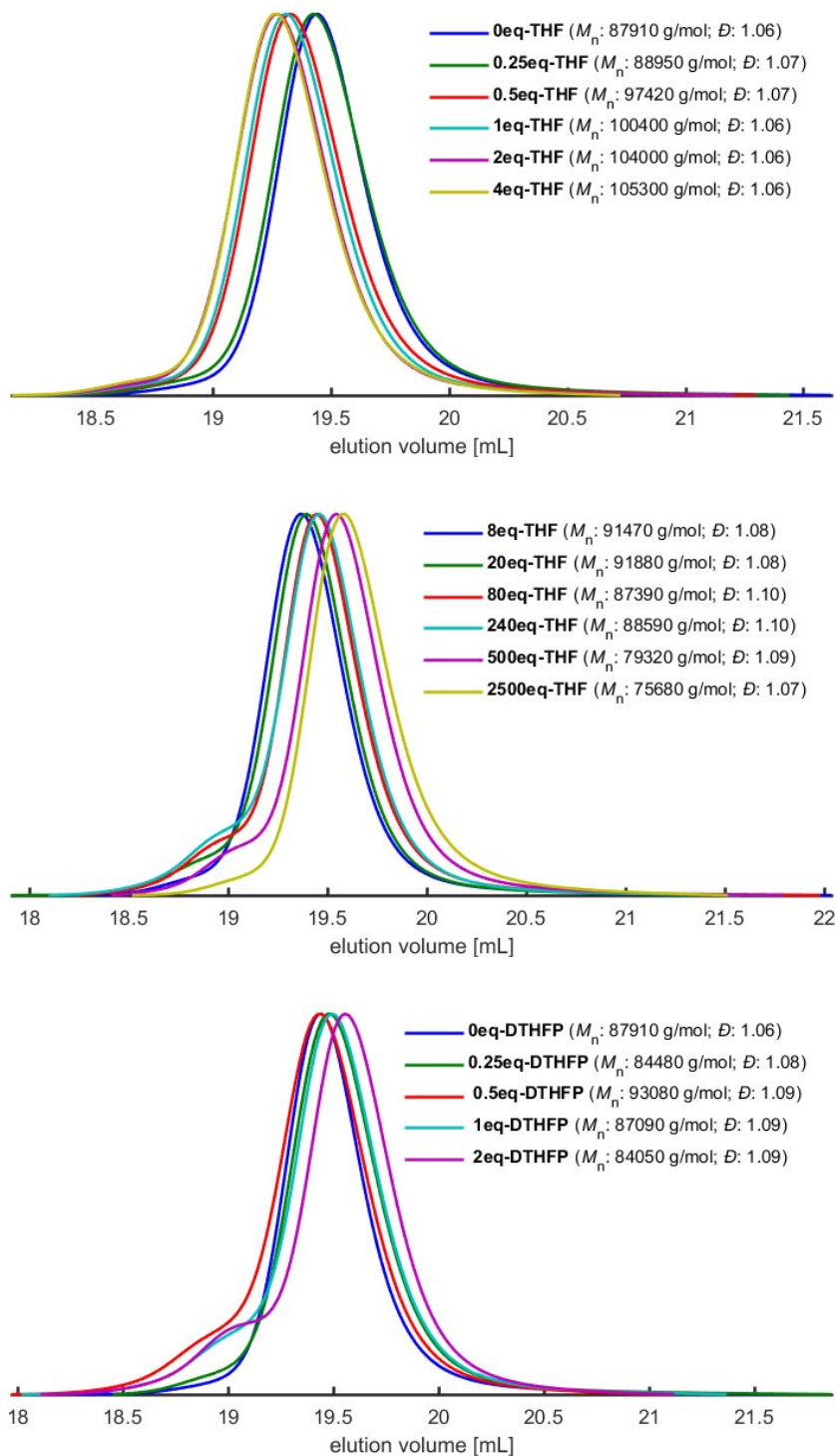


Figure S2: SEC traces of P(Myrc-co-S) copolymers synthesized with different modifier to Li^+ ratios.

Figure S2 and Table 1 show the results of the GPC analyses. Targeted molecular weight was 80 kg/mol, deviations are partially due to SEC-calibration with PS standards. It is known that the PS calibration overestimates the molecular weight of a PI sample by about 10%.² No literature values are available for PMyr. The elugrams show a narrow molecular weight distribution, as expected for a living polymerization. For some samples a shoulder can be seen at lower elution volumes, i.e. at higher molecular weights. This is explained by oxygen coupling during sampling.

4 Copolymerisation Kinetics and Determination of Reactivity Ratios

4.1 NIR spectra of reagents and solvents

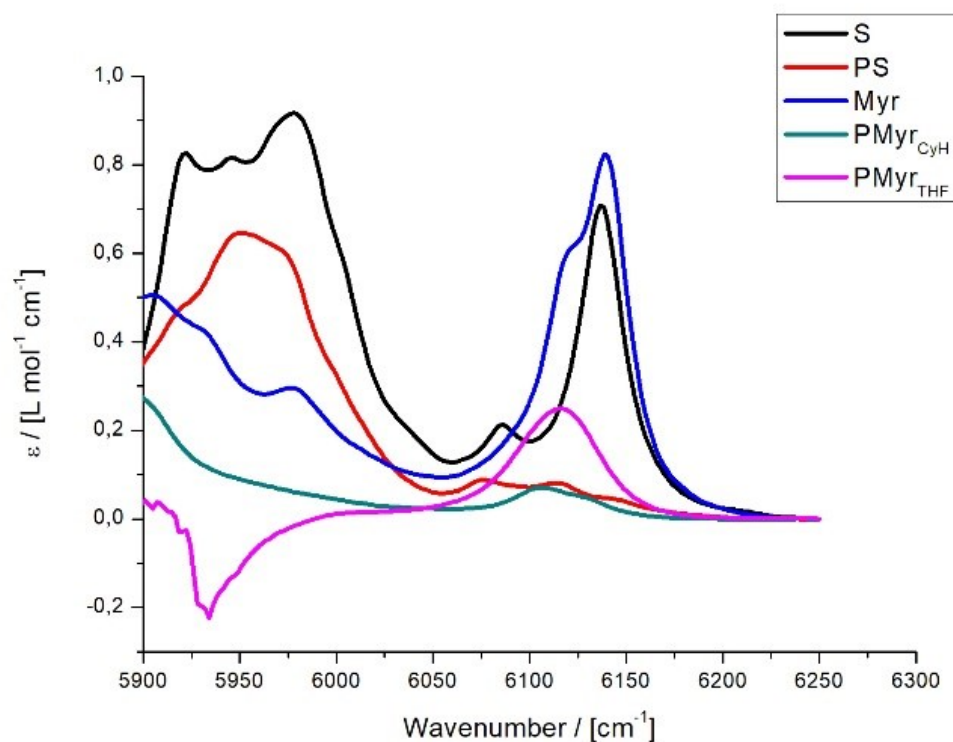


Figure S3: Molar attenuation coefficients of all species present in the reaction vessel during the polymerization: educts (S, Myr) and products (PS, PMyr_{CyH}, PMyr_{THF}). PMyr_{CyH} represents the molar attenuation coefficient of polymyrcene synthesized in cyclohexane (94% 1,4-units, 6% 3,4-units) and PMyr_{THF} the molar attenuation coefficient of polymyrcene synthesized in THF (36% 1,4-units, 51% 3,4-units and 13% 1,2-units). The negative absorbance of PMyr_{THF} in the wavelengths between 5900-5980 cm⁻¹ is explained by the absorbance of THF in this region.

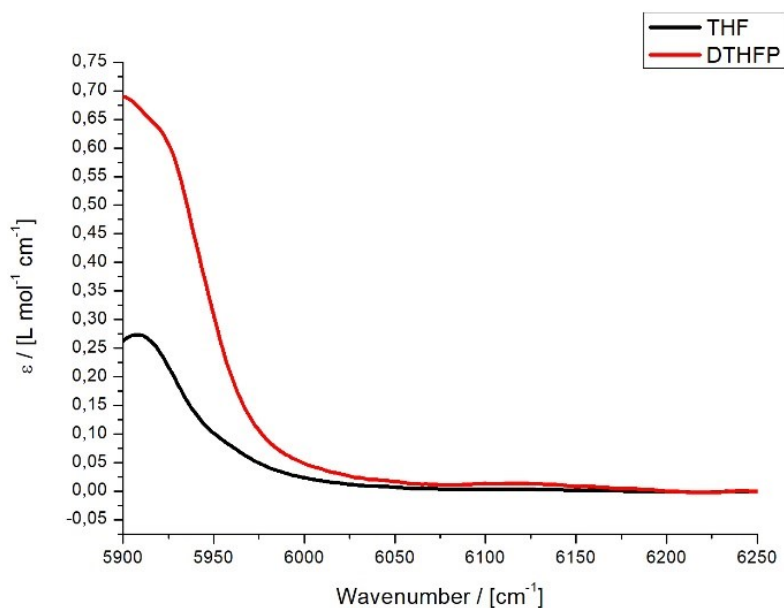


Figure S4: Molar attenuation coefficients of the modifiers THF and DTHFP.

4.2 Time-conversion plots

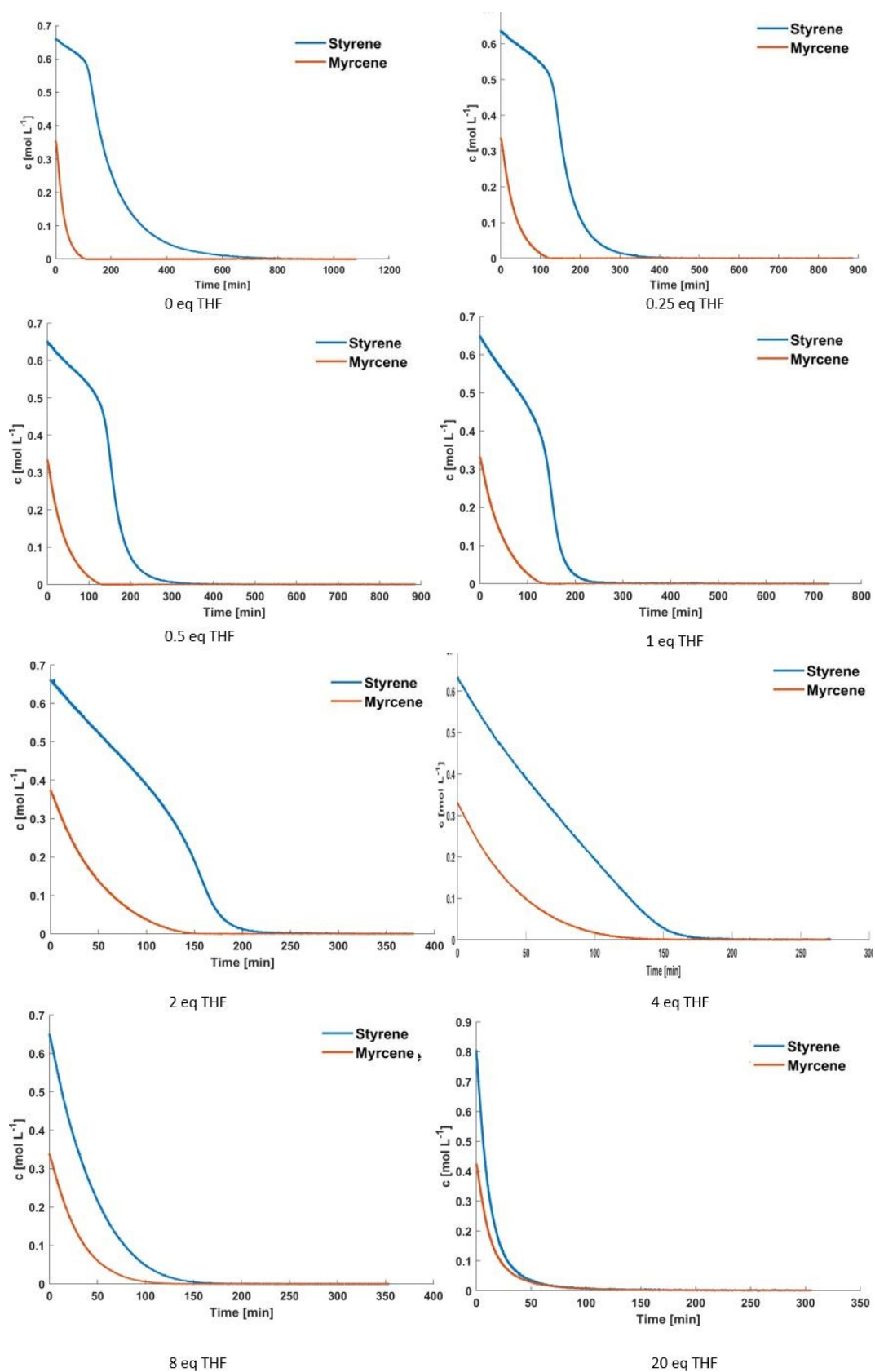


Figure S5a: Individual time-conversion plots at various THF contents

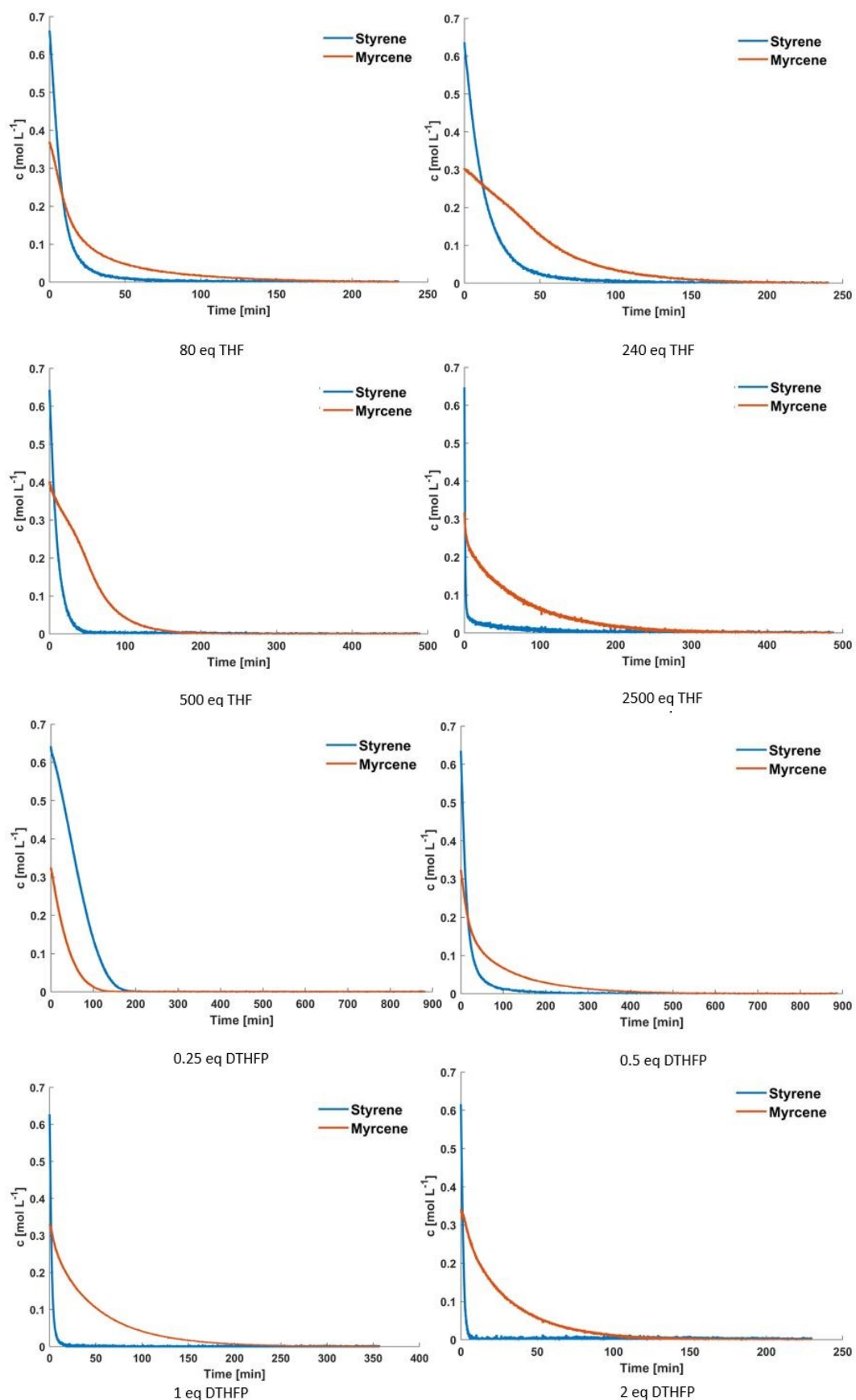


Figure S5b: Individual time-conversion plots at various contents of THF and DTHFP..

4.3 Individual monomer concentrations as a function of total conversion

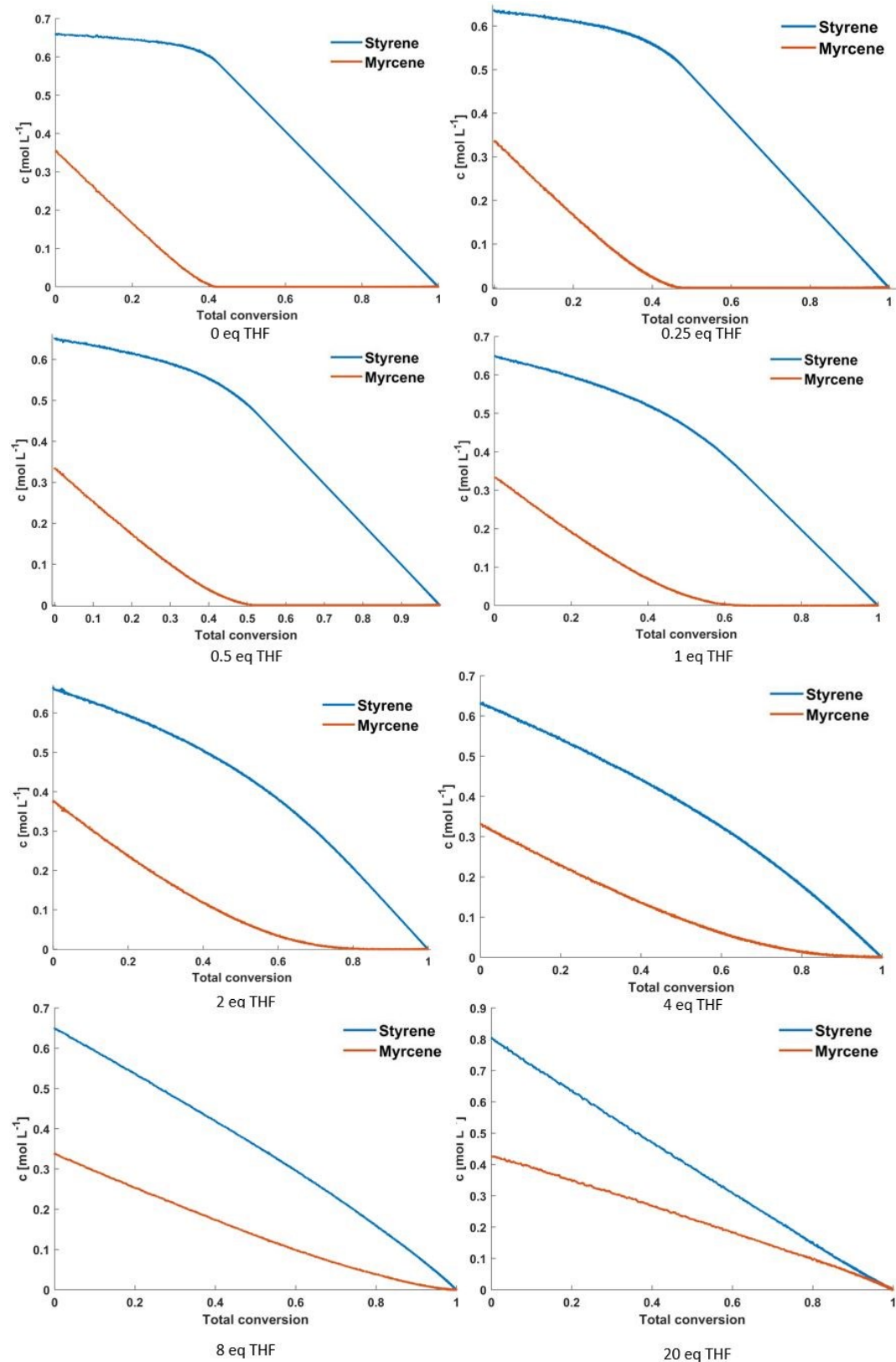


Figure S6a: Individual monomer concentrations as a function of total conversion various modifier contents.

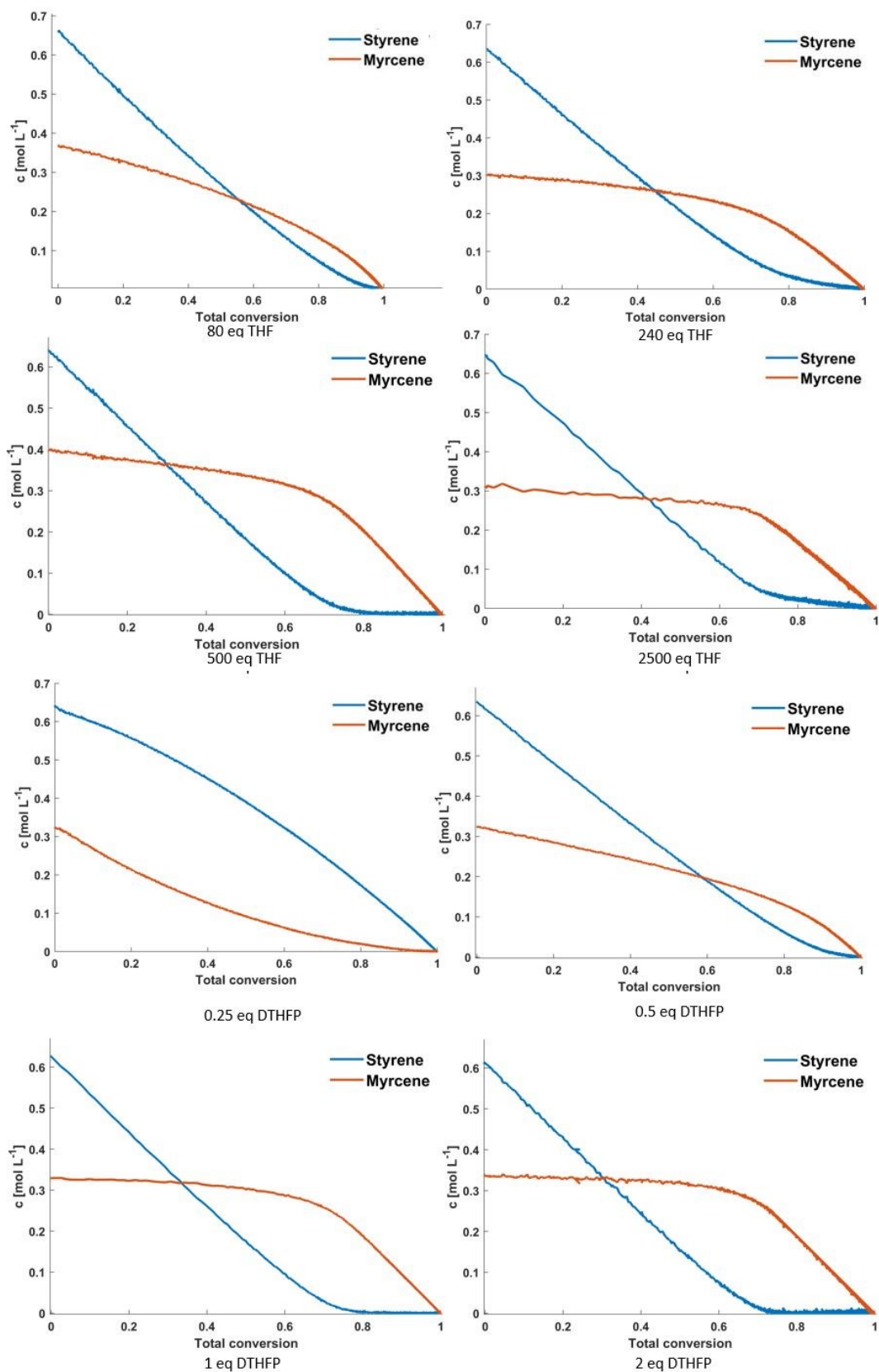


Figure S6b: Individual monomer concentrations as a function of total conversion at various modifier content.

4.4 Fits to determine reactivity ratios

The reactivity ratios r_{Myr} and r_S are determined by using three different equations: *Jaacks*, *Integrated Ideal* and *Beckingham-Sanoja-Lynd (BSL)*. These methods permit to calculate one reactivity ratio, and the other one is gained by assuming an ideal copolymerisation ($r_{Myr} \cdot r_S = 1$). The *Jaacks* equation^{6,7} was originally developed to simplify the Mayo-Lewis equation for the special case of an excess of one comonomer:

$$\log \frac{[M_1]_0}{[M_1]_t} = r_1 \log \frac{[M_2]_0}{[M_2]_t}$$

where $[M_1]_0$ and $[M_1]_t$ stand for the initial concentration of non-reacted monomer 1 and at time t , respectively. It can be shown that it is mathematically equivalent to the ideal case of the Meyer-Lowry equation.⁸

The *Integrated Ideal (Meyer-Lowry ideal)* method uses the integrated Skeist-equation for the non-terminal model:^{8,9,10}

$$X = 1 - \left(\frac{f_1}{f_{1,0}} \right)^{\frac{1}{r_1 - 1}} \left(\frac{1 - f_1}{1 - f_{1,0}} \right)^{\frac{r_1}{1 - r_1}}$$

where X represents the total comonomer conversion and $f_{1,0}$ and f_1 the initial mole fraction of monomer 1 and at a given time, respectively.

The *BSL Method* uses to following equations:^{11,12}

$$X = 1 - n_1(1 - p_1) - (1 - n_1)(1 - p_1)^{r_2}$$

$$X = 1 - n_2(1 - p_2)^{r_2} - (1 - n_2)(1 - p_2)$$

where p_A stand for the conversion of monomer A and n_A the mole fraction of monomer A at the beginning of the reaction.

The results are summarized in Table S1, and the individual fits can be seen in Figures S7-S9.

Table S1: Reactivity ratios (r_{Myr} and r_S) determined by the different nonterminal methods (*Jaacks*, *BSL* and *Ideal integrated (Meyer-Lowry Ideal)*) and their average for the copolymerisation at various $[modifier]/[Li]$ ratios.

[THF]/[Li]	r_S^{Jaacks}	r_{Myr}^{Jaacks}	r_S^{Ideal}	r_{Myr}^{Ideal}	r_S^{BSL}	r_{Myr}^{BSL}	r_S^{aver}	r_{Myr}^{aver}
0	0.024	41.1	0.024	42.5	0.024	38.3	0.024	40.6
0.25	0.049	20.6	0.047	21.2	0.049	19.6	0.049	20.5
0.5	0.082	12.2	0.075	13.4	0.082	11.3	0.082	12.3
1	0.15	6.79	0.14	7.17	0.15	6.57	0.15	6.85
2	0.23	4.40	0.23	4.38	0.23	4.35	0.23	4.38
4	0.40	2.52	0.39	2.55	0.40	2.48	0.41	2.56
8	0.64	1.56	0.64	1.56	0.64	1.55	0.64	1.56
20	1.14	0.88	1.13	0.89	1.15	0.87	1.15	0.87
80	2.11	0.47	2.13	0.47	2.19	0.47	2.18	0.46
240	5.73	0.18	5.71	0.18	5.86	0.17	5.77	0.17
500	7.99	0.13	8.59	0.12	7.20	0.13	7.92	0.12
2500	10.1	0.10	10.7	0.094	9.32	0.099	10.0	0.10
[DTHFP]/[Li]								
0.25	0.40	2.48	0.40	2.50	0.40	2.59	0.40	2.52
0.5	2.44	0.41	2.46	0.41	2.37	0.42	2.42	0.41
1	14.6	0.069	14.0	0.071	17.3	0.067	15.3	0.067
2	17.4	0.057	18.7	0.054	17.8	0.056	18.0	0.056

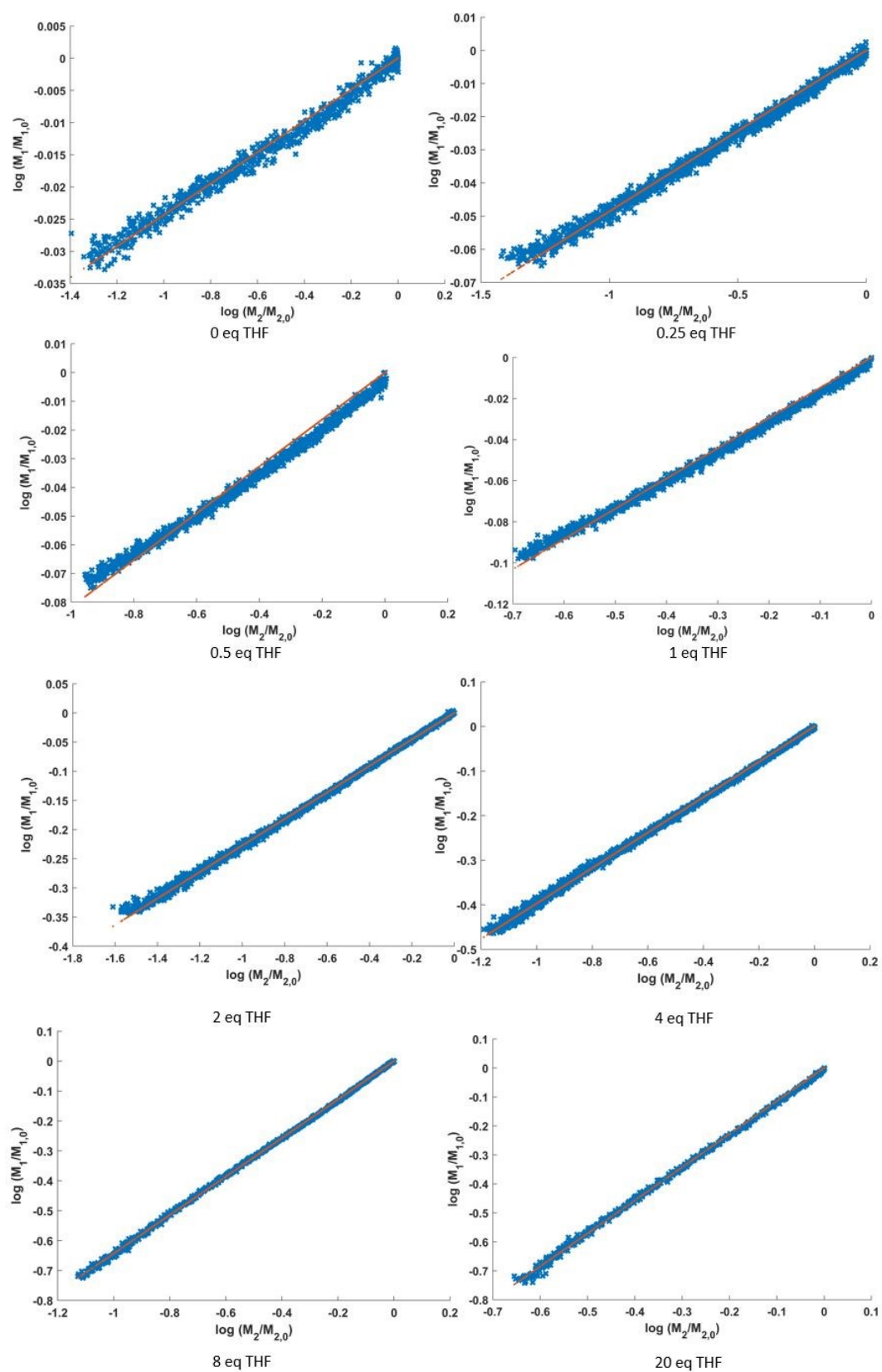


Figure S7a: Jaacks fits (red line) for the copolymerisation of Myr and S in the presence of various modifier contents. For all cases an excellent correlation between the red line and blue dots (experimental data) was found.

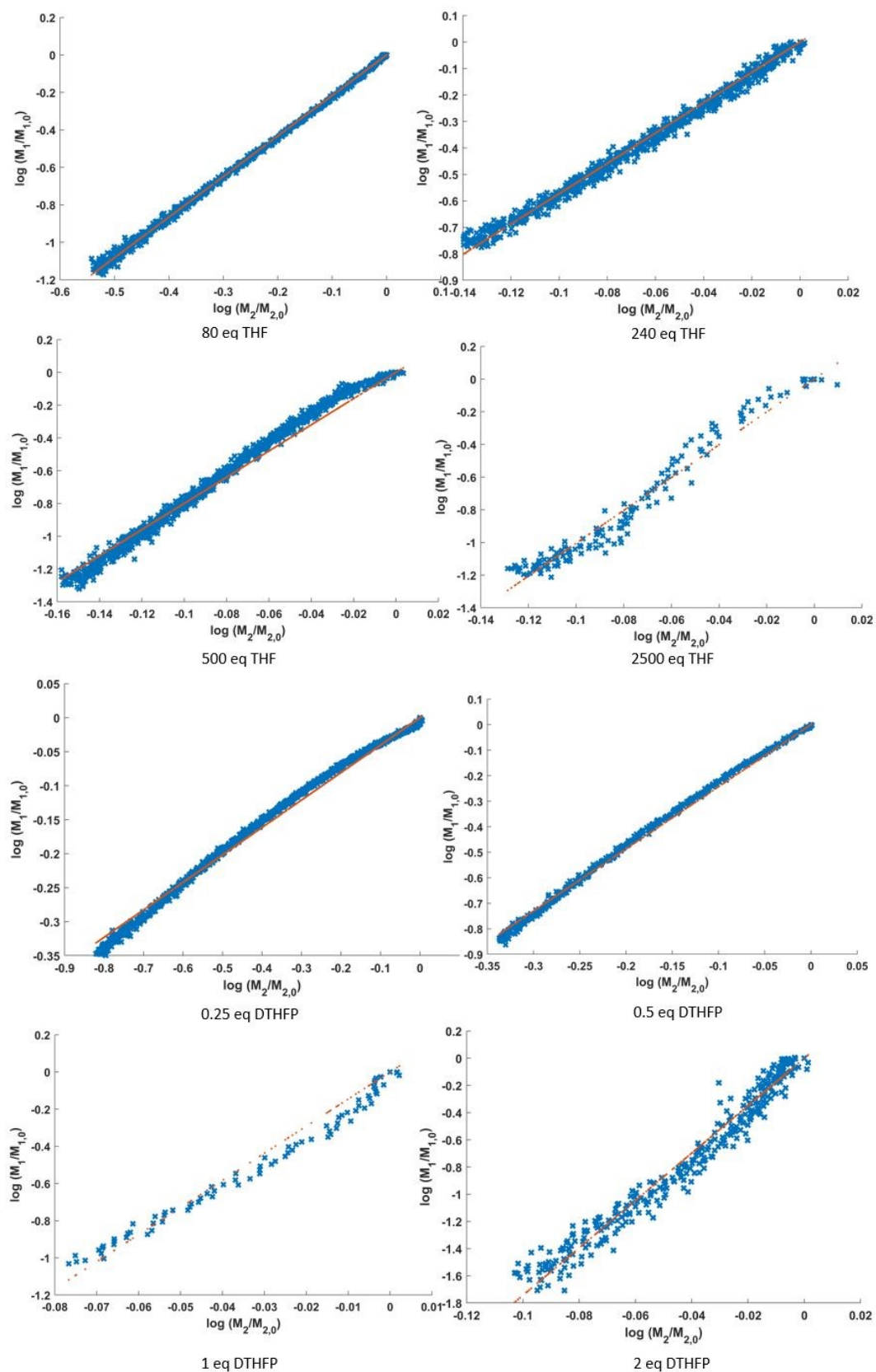


Figure S7b: Jaacks fits (red line) for the copolymerisation of Myr and S in the presence of various modifier contents. For all cases, an excellent correlation between the red line and blue dots (experimental data) was found.

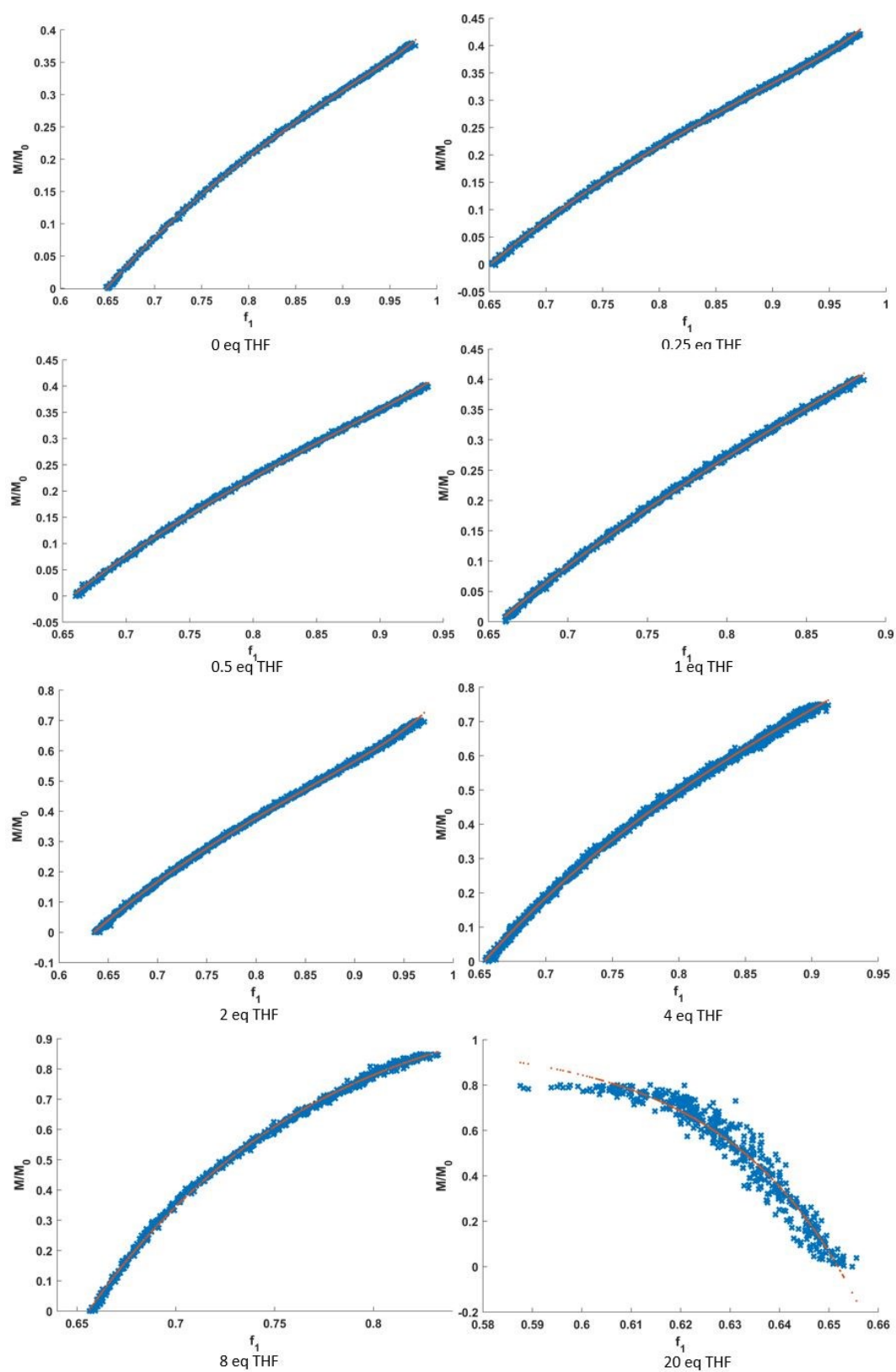


Figure S8a: Integrated ideal fits (red line) for the copolymerisation of Myr and S in the presence various modifier contents. The total monomer conversion is plotted against the mole fraction of styrene. For all cases, an excellent correlation between the red line and blue dots (experimental data) was found.

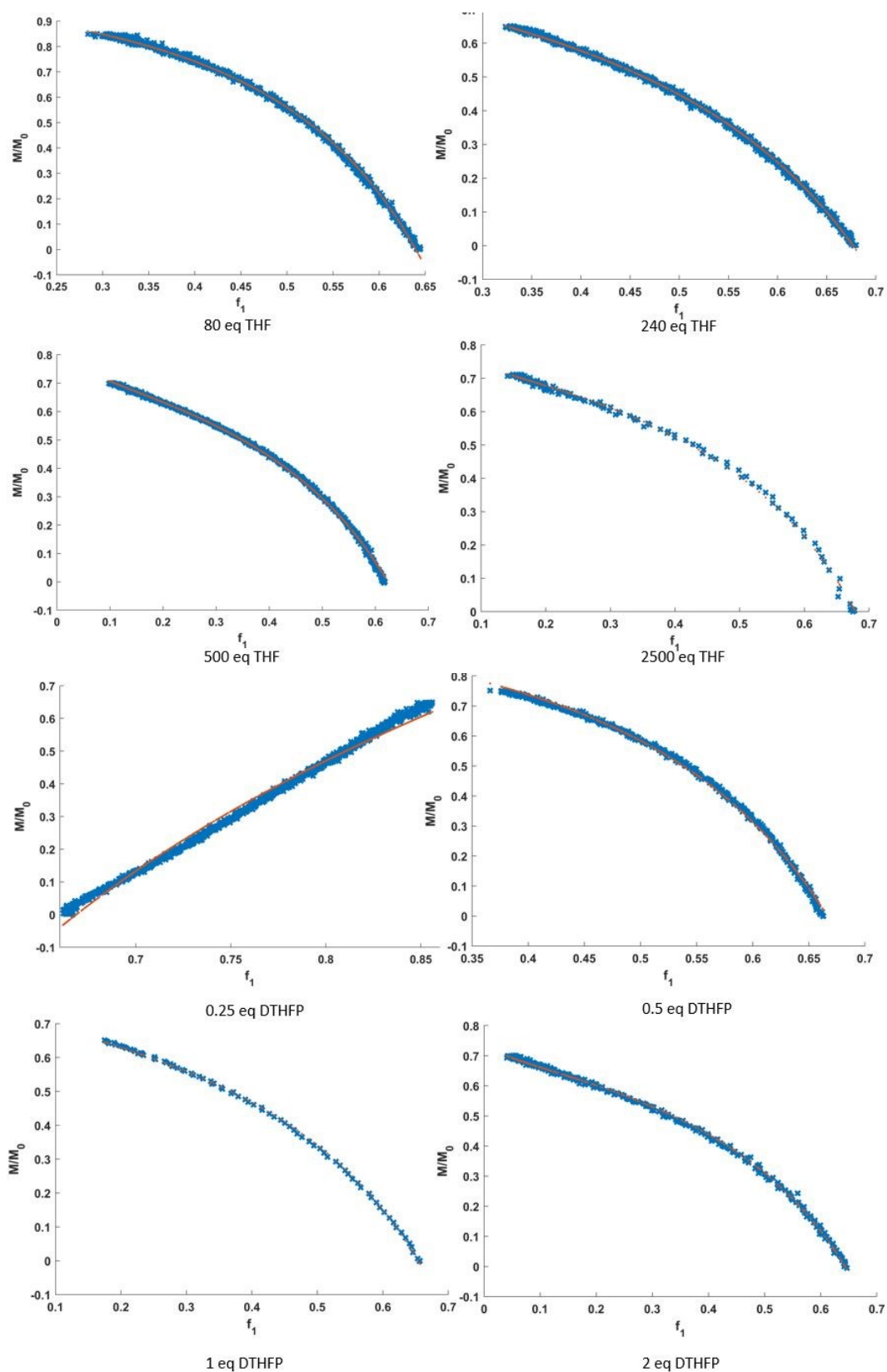


Figure S8b: Integrated (Meyer-Lowry) ideal fits (red line) for the copolymerisation of Myr and S in the presence of various modifier contents. The total monomer conversion is plotted against the mole fraction of styrene. For all cases, an excellent correlation between the red line and blue dots (experimental data) was found.

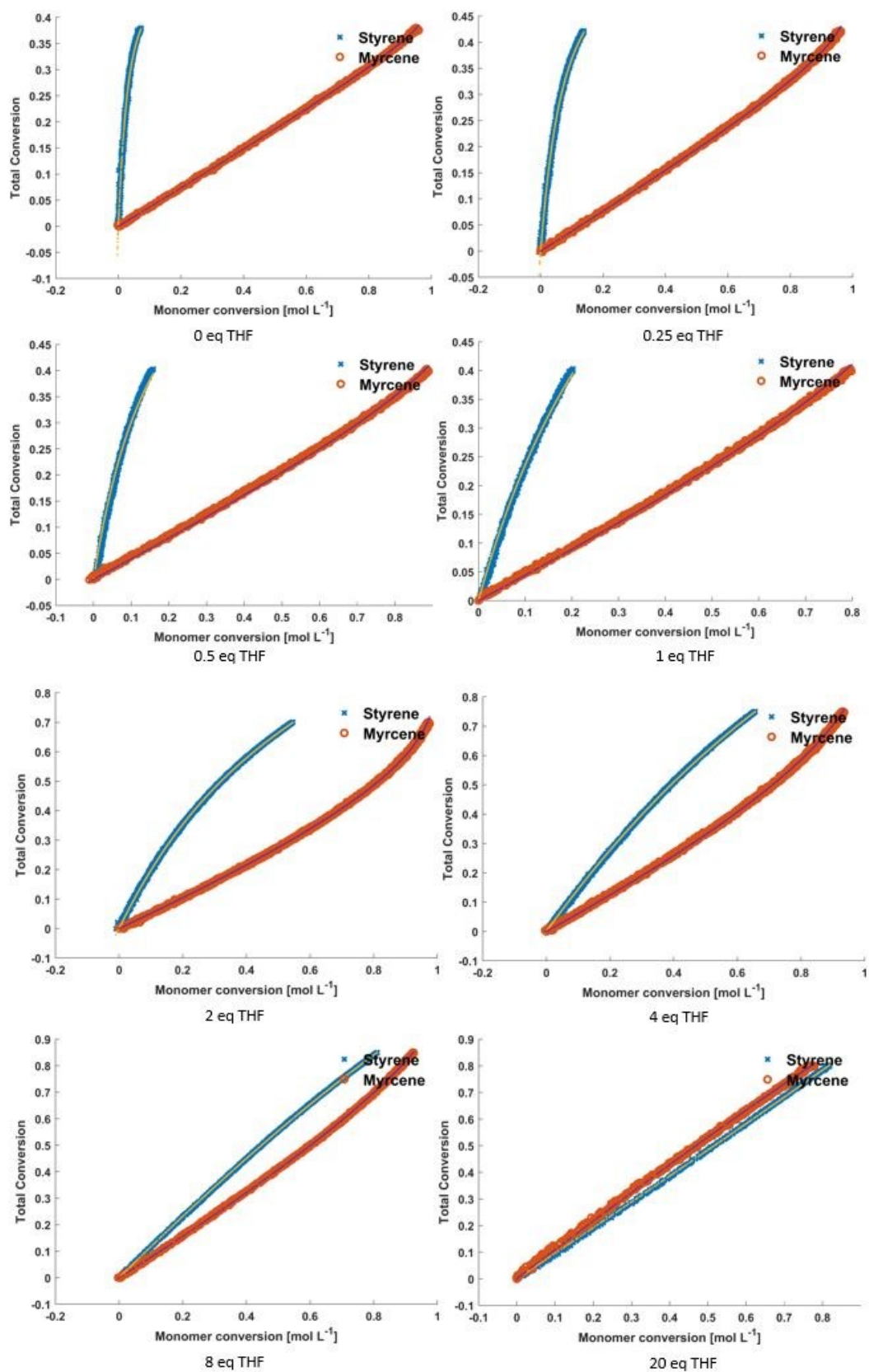


Figure S9a: BSL fits (blue and gold line) for the copolymerisation of Myr and S in the presence of various modifier contents. The total conversion is plotted against the monomer conversion. For all cases, an excellent correlation between experimental data (red and blue dots) and the fits was found.

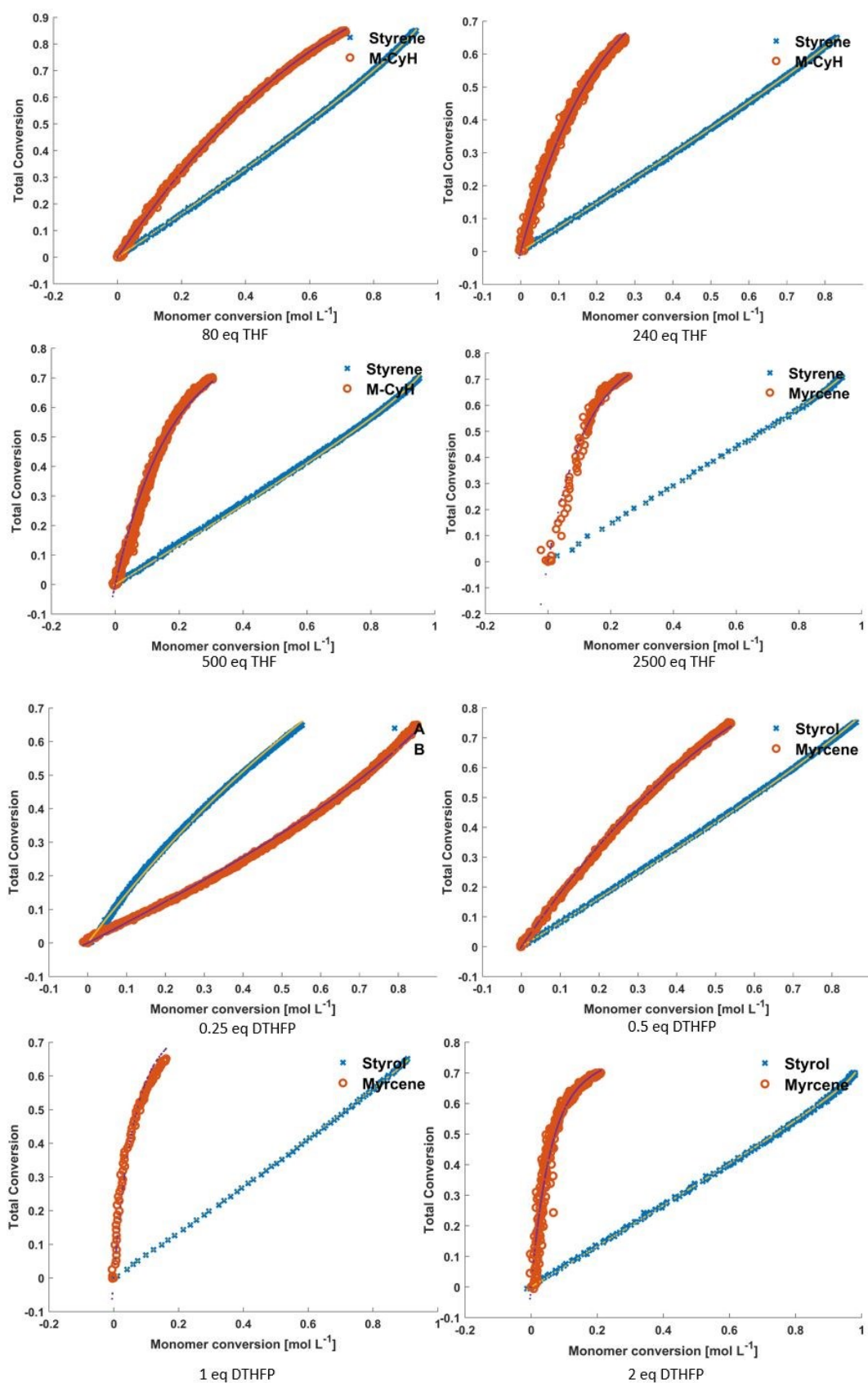


Figure S9b: BSL fits (blue and gold line) for the copolymerisation of Myr and S in the presence of various modifier contents. The total conversion is plotted against the monomer conversion. For all cases, an excellent correlation between experimental data (red and blue dots) and the fits was found.

5 Kinetics of Homopolymerisation of Myrcene

The homopolymerisation of myrcene in cyclohexane and THF was investigated (Figure S10) and compared to the homopolymerisation of isoprene and farnesene. For this purpose, pseudo-first-order plots are shown in Figure S11, where the slope represents the apparent rate constant, k_{app} .

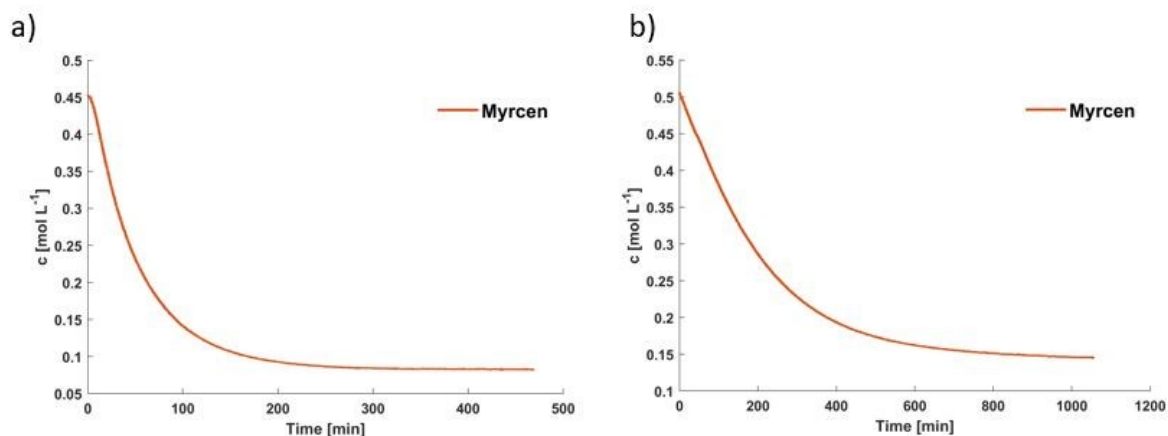


Figure S10: Time conversion plots for the homopolymerisation of myrcene in a) cyclohexane and b) THF at 20°C.

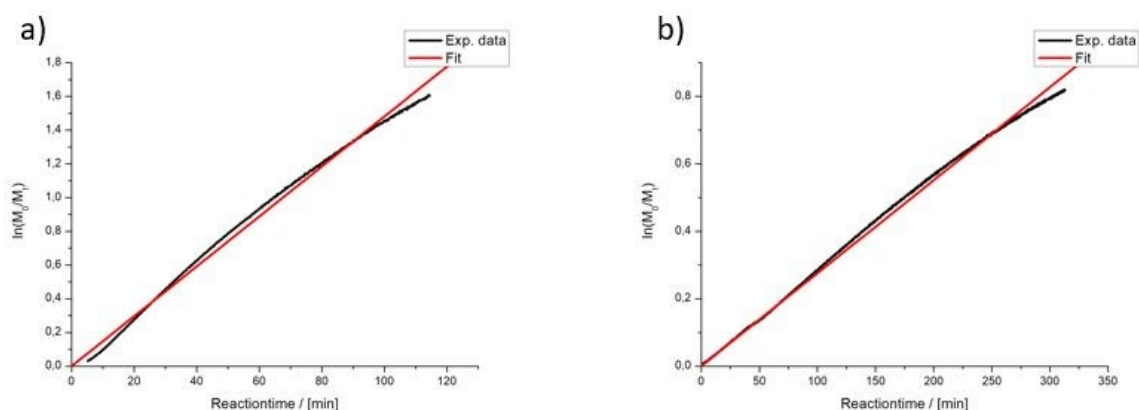


Figure S11: Pseudo-first order plots and linear fit of the homopolymerisation of myrcene in a) cyclohexane and b) THF.

To transform the obtained apparent rate constants, k_{app} , into the effective rate constant, k_p , it must be divided by the concentration of active chains. In THF the polymer chain ends are not aggregated, so k_{app} can be divided by the BuLi concentration. However, the aggregation number, N , of the PMyr-Li chain ends in cyclohexane is not known. Whereas for isoprene $2 \leq N \leq 4$ was observed, Schlaad *et al.* observed $N \approx 1$ in the nonpolar solvent limonene.¹³

Table S2 Apparent, k_{app} , and effective, k_p , rate constants for the homopolymerisation of isoprene, myrcene and farnesene.

Monomer	solvent	T °C	C_{ini} [mmol/L]	$10^3 k_{app}$ [s ⁻¹]	$10^{-3} k_p (N=4)$ [(L/mol) ^{1/4} s ⁻¹]	$10^{-3} k_p (N=1)$ [(L/mol) s ⁻¹]
Isoprene ¹⁴	CyH	20	1.17	0.092	0.50	-
Myrcene	CyH	20	0.77	0.245	1.47	318
Myrcene ¹³	limonene	23	13	0.30	-	23
Myrcene	THF	20	0.94	0.042	-	45
Farnesene ¹⁵	CyH	23	38	1.49	3.37	39

At comparable initiator concentration the apparent rate constant of myrcene in cyclohexane is six times higher than in THF. This is explained by the formation of a PMyr-Li chain end complex with THF, which has a lower reactivity. Assuming $N = 4$, the homopolymerization rate constant k_p in cyclohexane is between the ones of isoprene¹⁴ and farnesene¹⁵. This is explained by the sterically demanding sidechain likely to reduce the aggregation number. Assuming $N = 1$, k_p in cyclohexane is one magnitude higher than that of farnesene and that determined by Schlaad et al. in limonene, indicating that the aggregation behaviour in cyclohexane may differ from that in limonene. The association behaviour of myrcene in cyclohexane is a matter of future investigations.

Half-lives of Myr and S in the copolymerizations were determined from the time-conversion plots (Fig. S5) and are compared to those of the copolymerisation of styrene and isoprene in cyclohexane (20°C) in the presence of THF as modifier.¹⁶ The comparison of the relative half-lives is shown in Table S3 and Figure S12.

Table S3: Half-lives of the copolymerization of styrene with myrcene, of the comonomers as a function of the [modifier]/[Li] ratio used. For comparison, the half-lives of the copolymerization of styrene with isoprene are also shown.²

[THF]/[Li]	$t_{1/2,Myr}$ / [min]	$t_{1/2,S}$ / [min]	$t_{1/2,I}$ / [min] ¹⁶	$t_{1/2,S}$ / [min] ¹⁶
0	22	167	120	720
0.25	24	149	120	520
0.5	28	149	120	420
1	31	135	100	220
2	39	111	75	130
4	28	59	47	55
8	21	29	31	32
20	13	11	18	14
80	13	5.5	12	5.5
240	36	8.2	23	7.4
500	53	6.4	30	5.8
2500 ^a	(22)	(0.7)	(16)	(0.8)
[DTHFP]/[Li]				
0.25	27	56	-	-
0.5	22	8.8	-	-
1	24	1.5	-	-
2	16	1.0	-	-

^aData points are unreliable due to strong exothermicity.

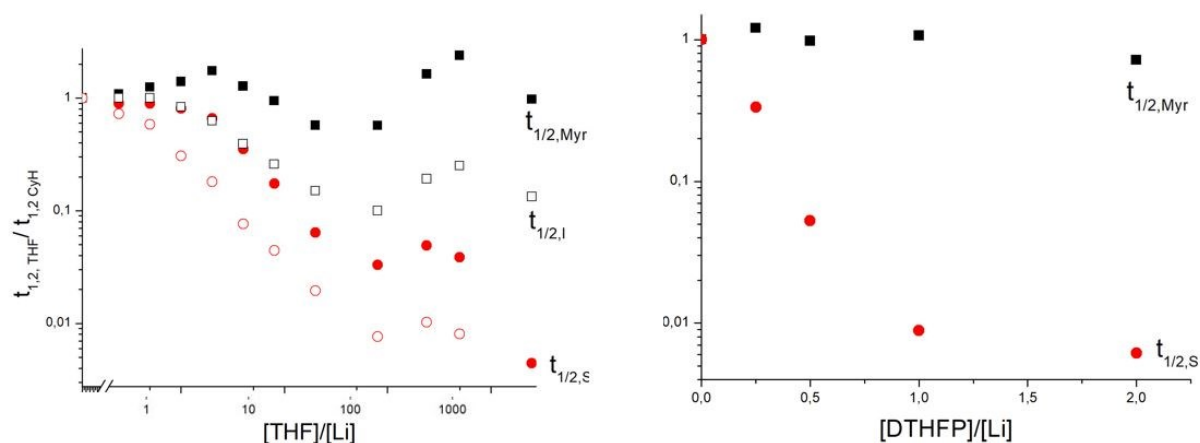


Figure S12: Half-lives of comonomers in the copolymerisation of styrene with myrcene relative to the half-lives in pure cyclohexane. For comparison, the relative half-lives of the copolymerisation of styrene with isoprene are shown.²

For the ligand THF the half-lives of the comonomers relative to the half-lives in pure cyclohexane show a distinct minimum at $[\text{THF}]/[\text{Li}] \approx 80$, corresponding to a maximum of the polymerization rate. The effect is much stronger for styrene than for myrcene. To a somewhat larger extent this effect was already observed in the copolymerization of S and I. The increase of the rate was already explained by a shift of the dissociation/complexation equilibria of the chain end with several THF ligands (Scheme 1).^{2,17,18} For $[\text{THF}]/[\text{Li}] = 2500$, the half-life of myrcene decreases (rate increases) again. This could be related to the significantly increased reaction temperature due to the very rapid and exothermic polymerization.¹⁴

For DTHFP as Lewis base, the half-life of myrcene does not change significantly, and for styrene it decreases with increasing modifier content (i.e. with increasing polymerization rate), as expected. Since DTHFP is a chelating ligand only one molecule fits to the Li ion at the chain end. Thus, the monoadduct/diadduct equilibrium is not present.

6 Copolymer composition

6.1 Volume composition profiles

The molar composition diagrams calculated from the reactivity ratios are shown in Figure 2. For the discussion of the morphologies, volume-related diagrams are necessary. For this purpose both axes are weighted by the molecular weight and the density of the repeating unit.¹⁹ The used homopolymer densities are $\rho_{\text{PMYr}} = 0.892 \text{ g/cm}^3$ and $\rho_{\text{PS}} = 1.05 \text{ g/cm}^3$.²⁰

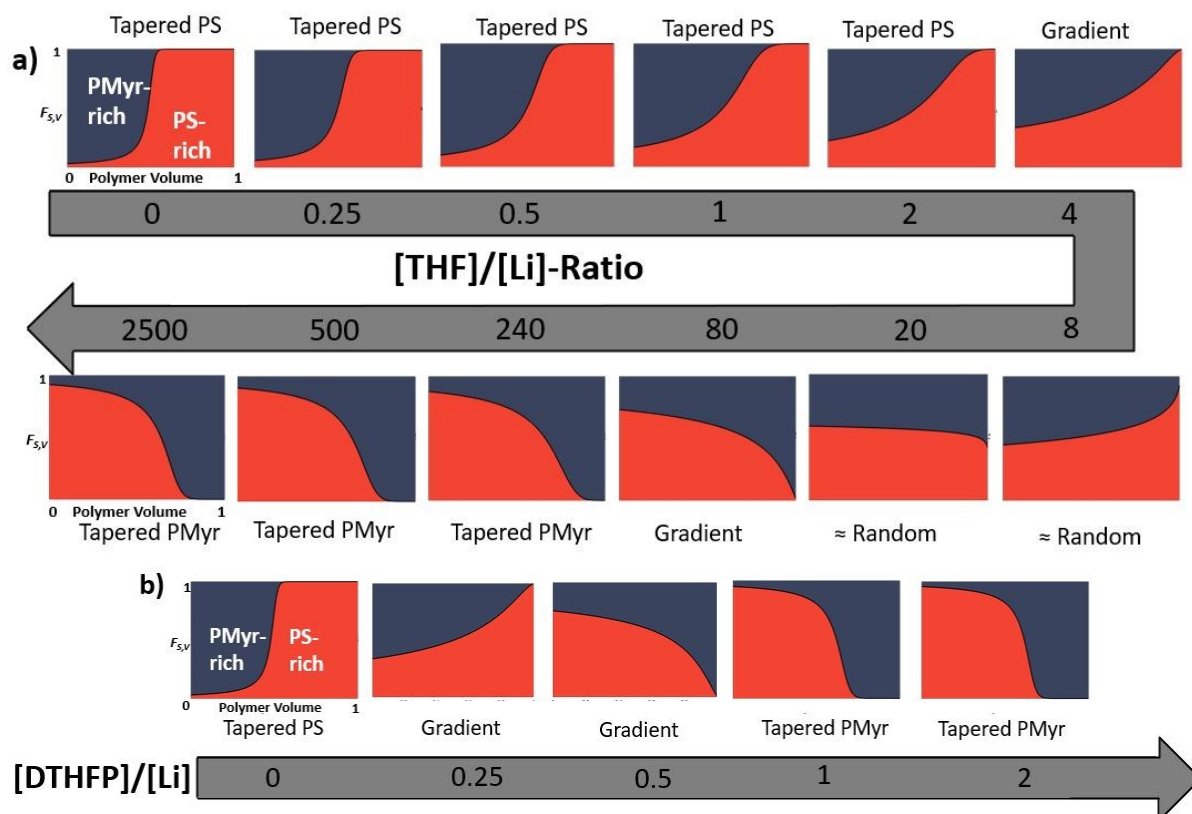


Figure S13: Volume composition profile of the copolymer $P(\text{Myr-co-S})$ in dependence of the used $[\text{modifier}]/[\text{Li}]$ ratio (a) THF; b) DTHFP), presented by the instantaneous styrene volume incorporation ($F_{s,v}$) as a function of the polymer volume.

6.2 Blockiness

The so called “blockiness” of the styrene units in the copolymer was investigated using $^1\text{H-NMR}$ spectroscopy (Fig. S18-S22). For the determination of this parameter the aromatic signals of the styrene units are considered. The $^1\text{H-NMR}$ signals of the h protons (Fig. S18-S22) broaden due to the spatial presence of other styrene units.²¹ When a magnetic field acts on the six π -electrons of the phenyl ring, this induces a ring current enhancing the applied field at the edges of the ring where the ring protons are located. Thus, their resonance is observed at lower shifts. This is true for all protons of the phenyl ring, but especially for those of the *ortho*-protons, which are located closer to the faces of neighboring rings than the *meta*- and *para*-protons. They therefore appear more strongly shifted low-field. In this case, when the styrene sequence is long, a separate signal is observed; if the styrene sequence is shorter, the *ortho*-H signal appears broadened or as a shoulder of the main aromatic signal. At $[\text{THF}]/[\text{Li}] = 0$, the two aromatic signals (i+j and h) are resolved and appear separately. With increasing THF content up to 20 equivalents the h signal is increasingly high-field shifted and partially merges with the i+j signal. With further increasing THF equivalents, the signals separate again. This

confirms that an almost random copolymer is present at 8 and 20 eq THF. V.D. Mochel was able to show that the necessary styrene block length for the application of this method must be at least two or three units.²² To calculate the blockiness B , the ratio of the integrals between 7.43-6.35 ppm, I_1 (5 protons), and from 6.89-6.35 ppm, I_2 (2 protons), are used:²

$$B = \frac{I_1/5}{I_2/2}$$

Furthermore, the average number of styrene units, N_s , per styrene block is related to the blockiness by:²³

$$B = \frac{N_s}{N_s + 2}$$

$$N_s = \frac{2B}{1 - B}$$

The results are shown in Table S4. The minimum of block structures ($N_s = 3.3-3.4$) is found between 8 and 20 eq THF, which agrees with the near-random composition determined from the reactivity ratios (see Table 1 and Figure 2). Assuming that two consecutive styrene units ($N_s = 2$) can already be recognized as a block,²² the minimum achievable blockiness is 50%. For $[THF]/[Li] = 0$, $N_s = 15$, resulting from one very long PS block and many very short sequences interrupting the long series of myrcene units. For $[THF]/[Li] \geq 500$ longer styrene sequences are formed than for $[THF]/[Li] = 0$. Here, long styrene sequences are interrupted by single myrcene units.

Table S4: Average number of connected styrene units, N , and blockiness.

[THF]/[Li]	Blockiness / [%]	N_s
0	88	15
0.25	86	12
0.5	83	9.8
1	78	6.9
2	70	4.7
4	66	3.9
8	63	3.4
20	62	3.3
80	76	6.3
240	89	16
500	92	23
2500	98	98
[DTHFP]/[Li]		
0.25	74	5.8
0.5	80	8.0
1	93	27
2	95	38

7 Microstructure of the Myrcene Units

For the determination of the microstructure of the myrcene units $^1\text{H-NMR}$ spectroscopy is used. The following Figures show the $^1\text{H-NMR}$, $^{13}\text{C-NMR}$ and 2D spectra of the homopolymer polymyrcene prepared in pure cyclohexane and in THF.

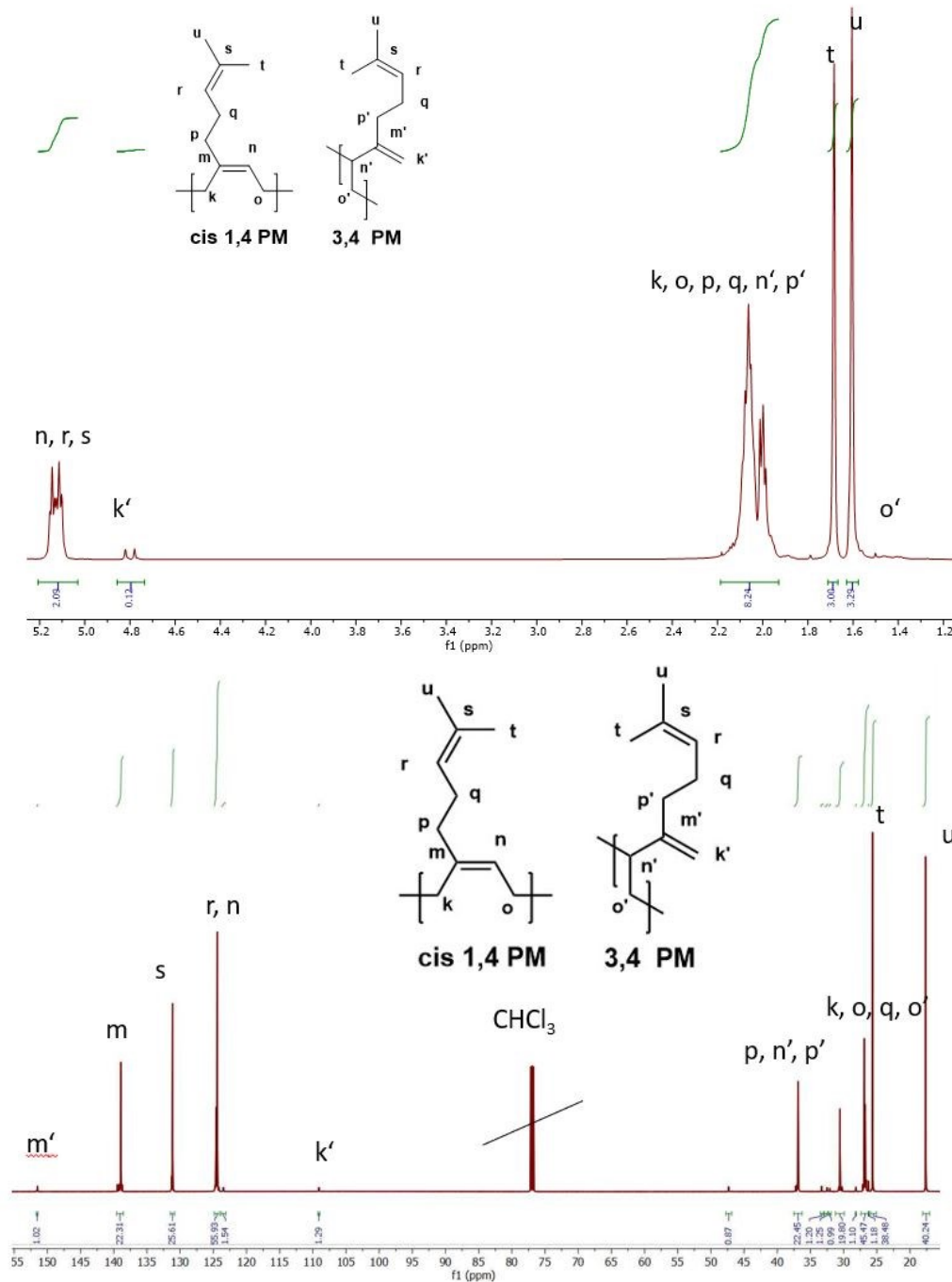
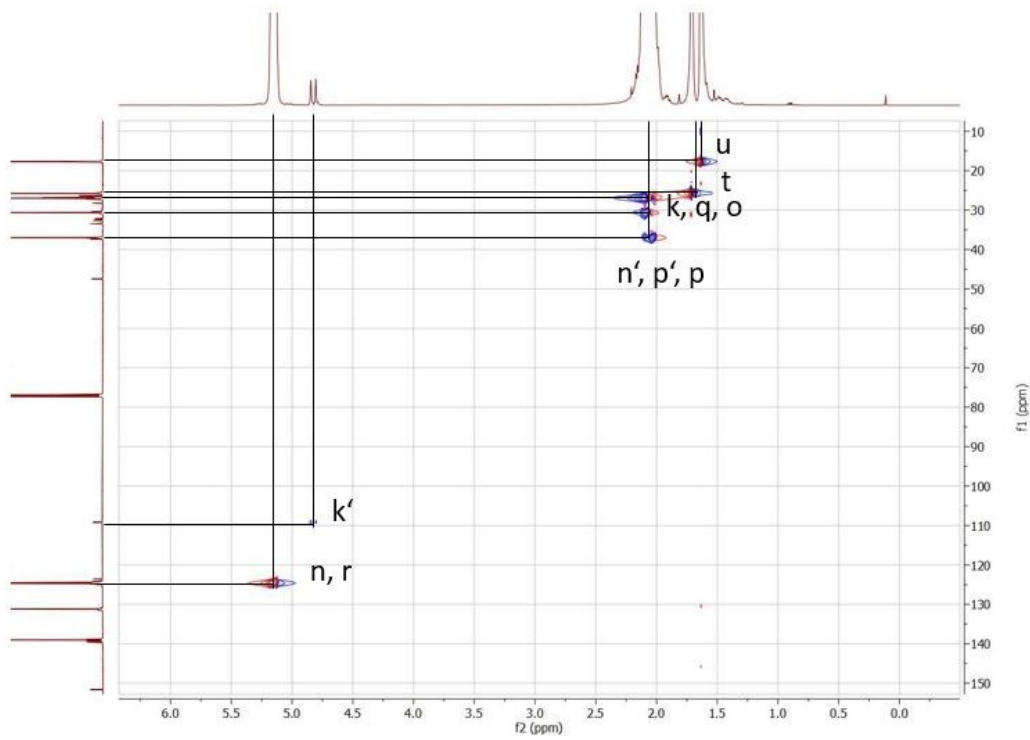
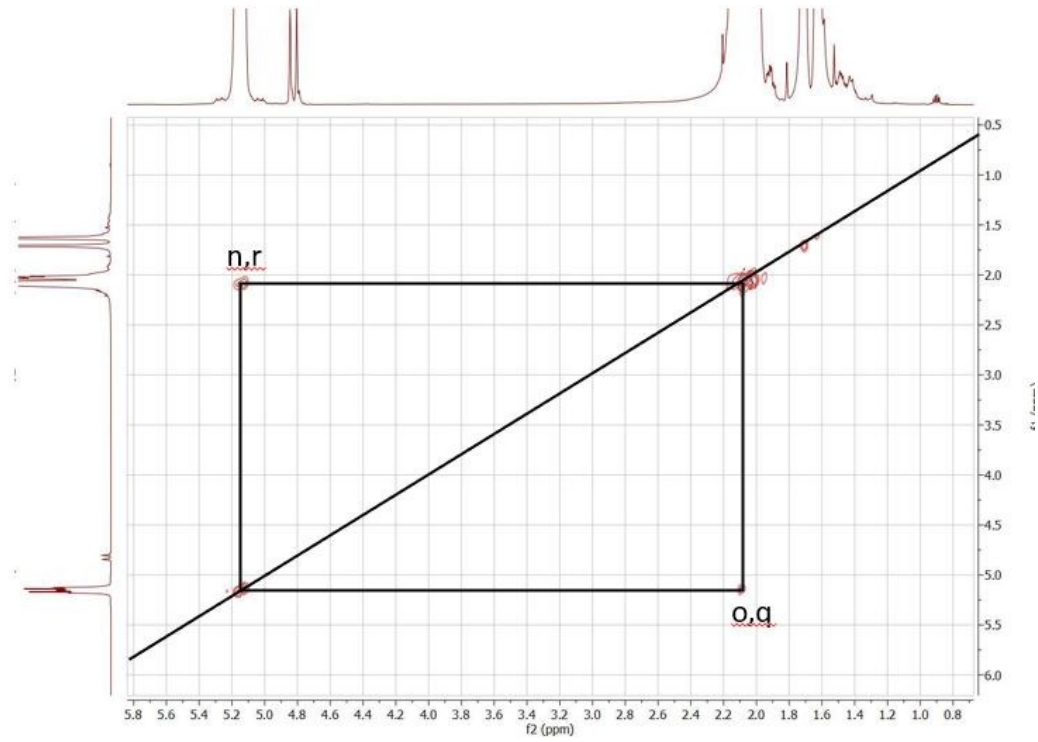


Figure S14: Assigned $^1\text{H-}$ and $^{13}\text{C-NMR}$ signals of polymyrcene synthesized in cyclohexane.

^1H : (CDCl_3 , 600 MHz, δ ppm): 5.19-4.98 (n, r); 4.94-4.59 (k'); 2.18-1.79 (k, o, p, q, n', p'); 1.68 (t); 1.62 (u); 1.52-1.35 (p')

^{13}C : (CDCl_3 , 151 MHz, δ ppm): 151 (m'); 138 (m); 131 (s); 124 (r, n); 109 (k'); 37 (p, n', p'); 30-26 (k, o, q, o'); 25 (t); 18 (u)



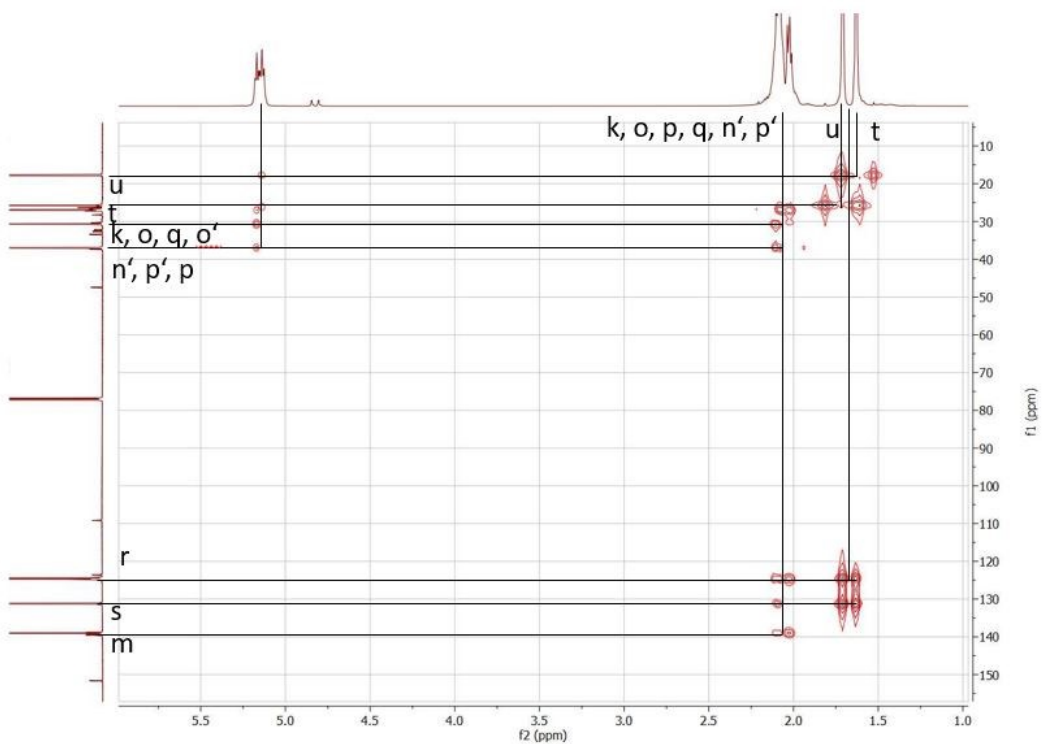


Figure S15: COSY, HSQC and HMBC spectra of polymyrcene synthesized in cyclohexane.

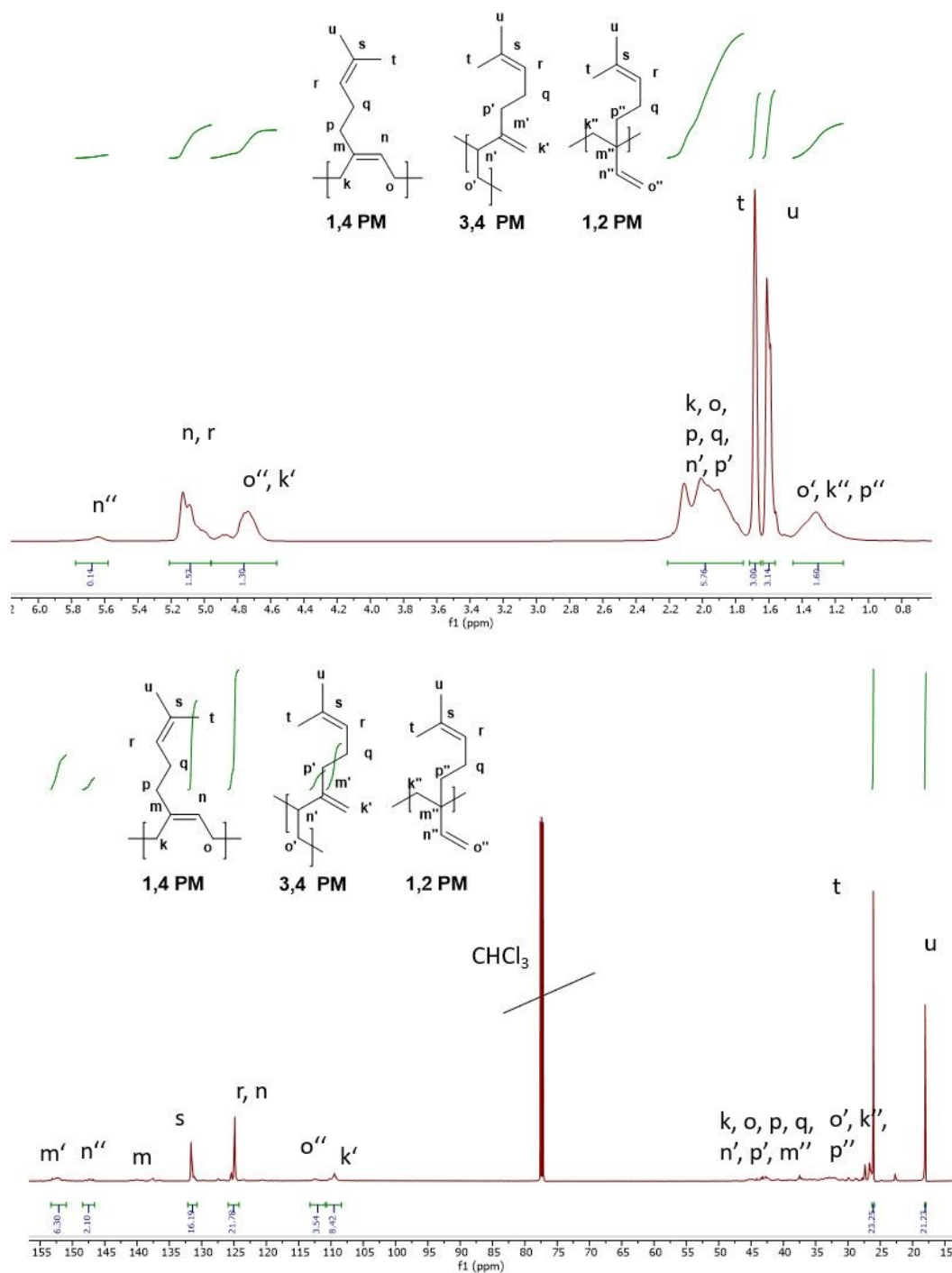
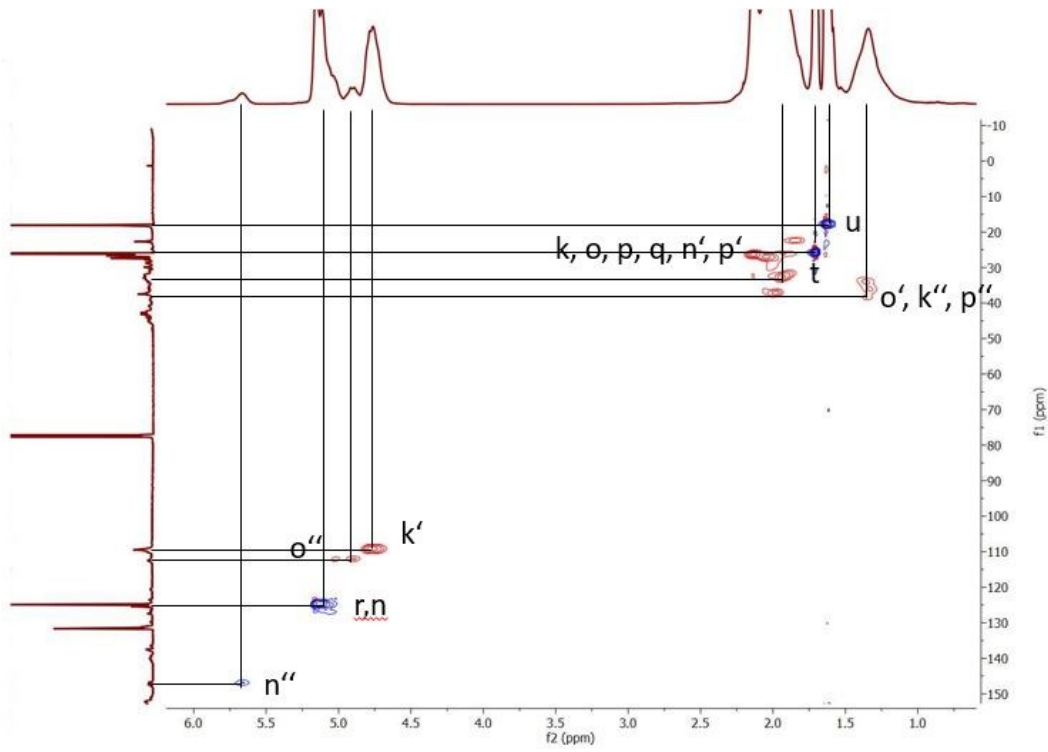
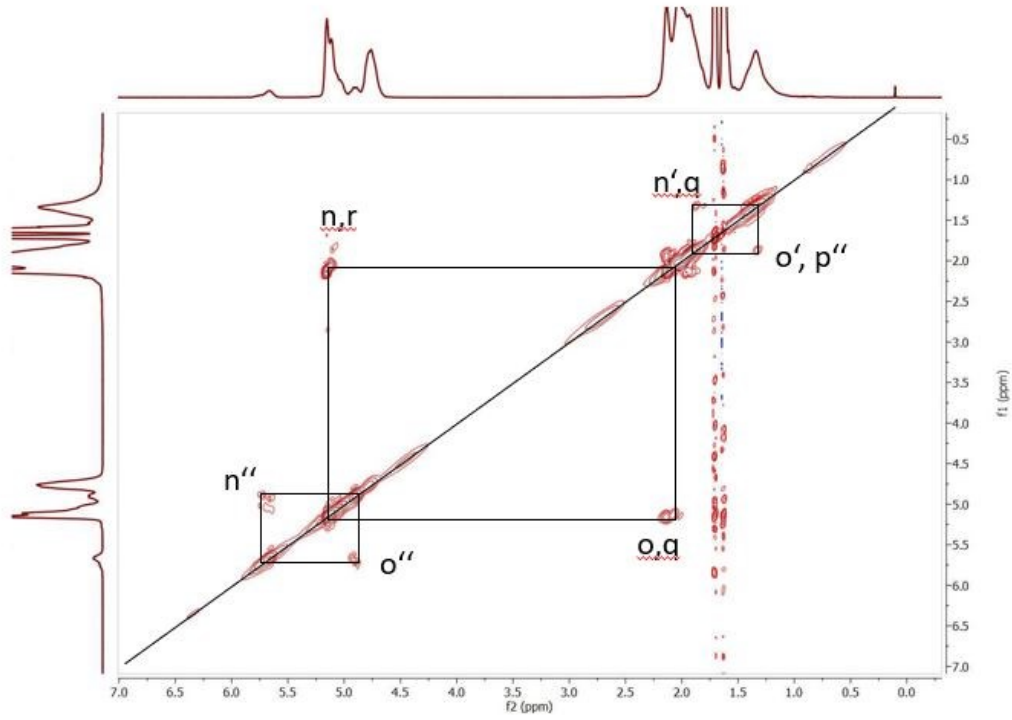


Figure S16: Assigned ^1H - and ^{13}C -NMR signals of polymycene synthesized in THF.

The assignment of the peaks is:

^1H : (CDCl_3 , 600 MHz, δ ppm): 5.76-5.56 (n''); 5.19-4.98 (n, r); 4.94-4.59 (k', o''); 2.18-1.79 (k, o, p, q, n', p'); 1.68 (t); 1.62 (u); 1.52-1.35 (p', k'', p'')

^{13}C : (CDCl_3 , 151 MHz, δ ppm): 151 (m'); 147 (n''); 138 (m); 131 (s); 124 (r, n); 112 (o''); 109 (k'); 45-35 (k, o, p, q, n', p', m''); 35-26 (o', k'', p''); 25 (t); 18 (u)



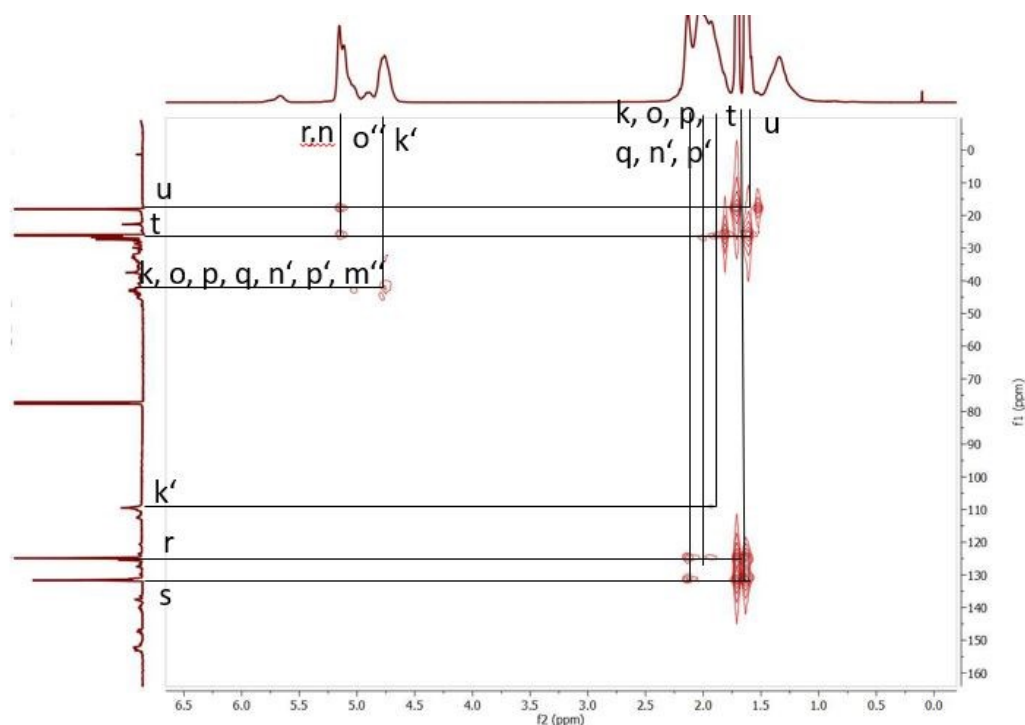
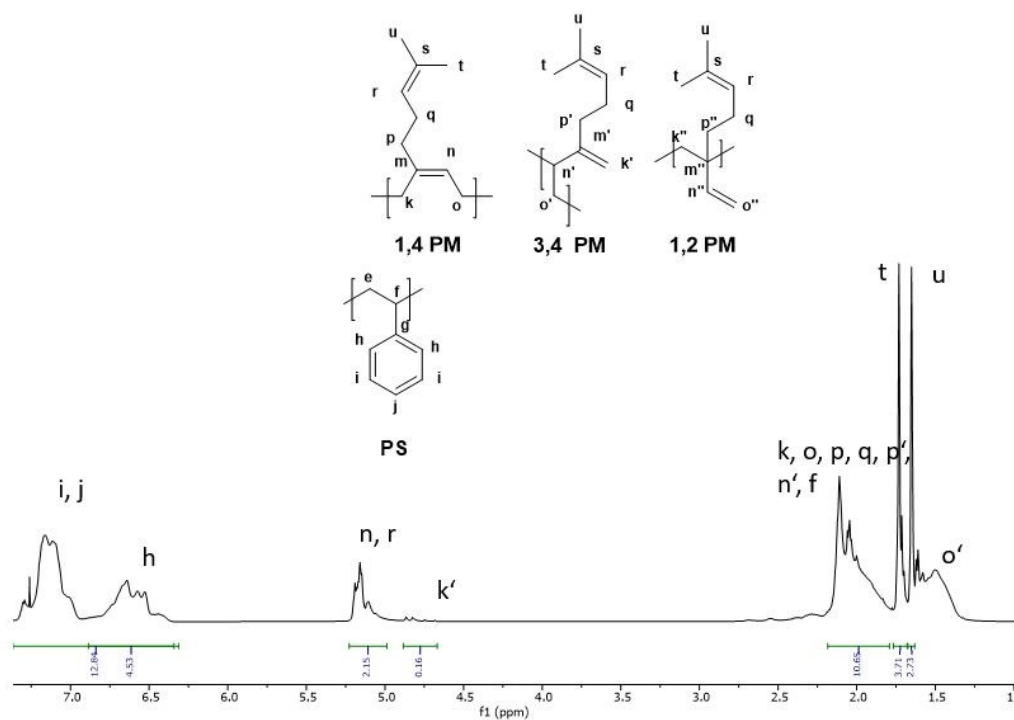


Figure S17: COSY, HSQC and HMBC spectra of polymycene synthesized in THF.

The ^1H - and $^{13}\text{C}_{\text{ig}}$ -NMR and 2D analytics (COSY, HSQC and HMBC) of the copolymers P(Myrc-co-S) synthesized with 0 and 2500 eq THF are shown in the following Figures.

The assignment of the different signals is impeded by the numerous overlapping signals of the different microstructures of polymycene. The copolymerization of myrcene with styrene makes the spectra even more complex, as the styrene signals additionally split due to the styrene triads.



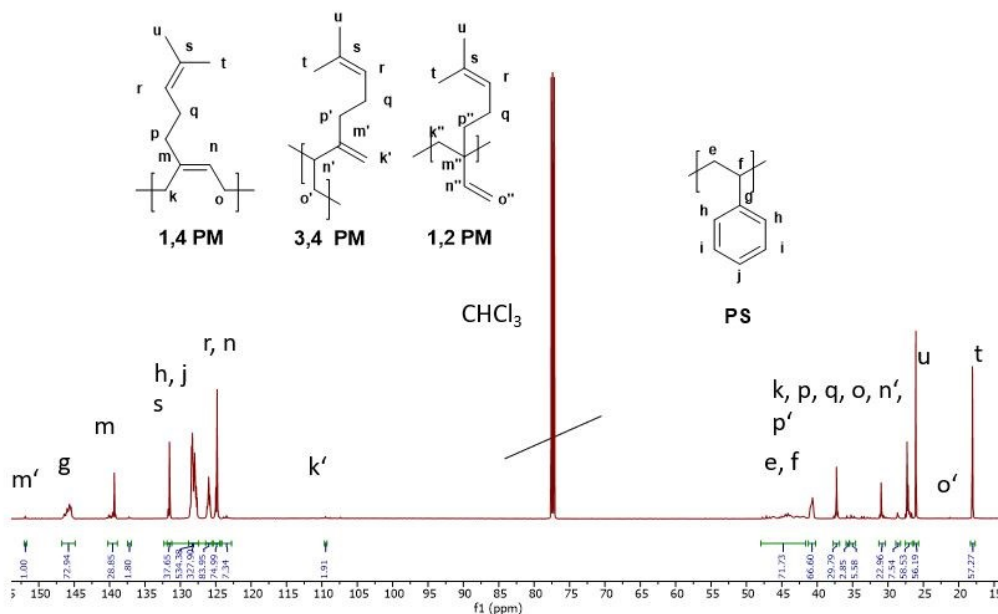
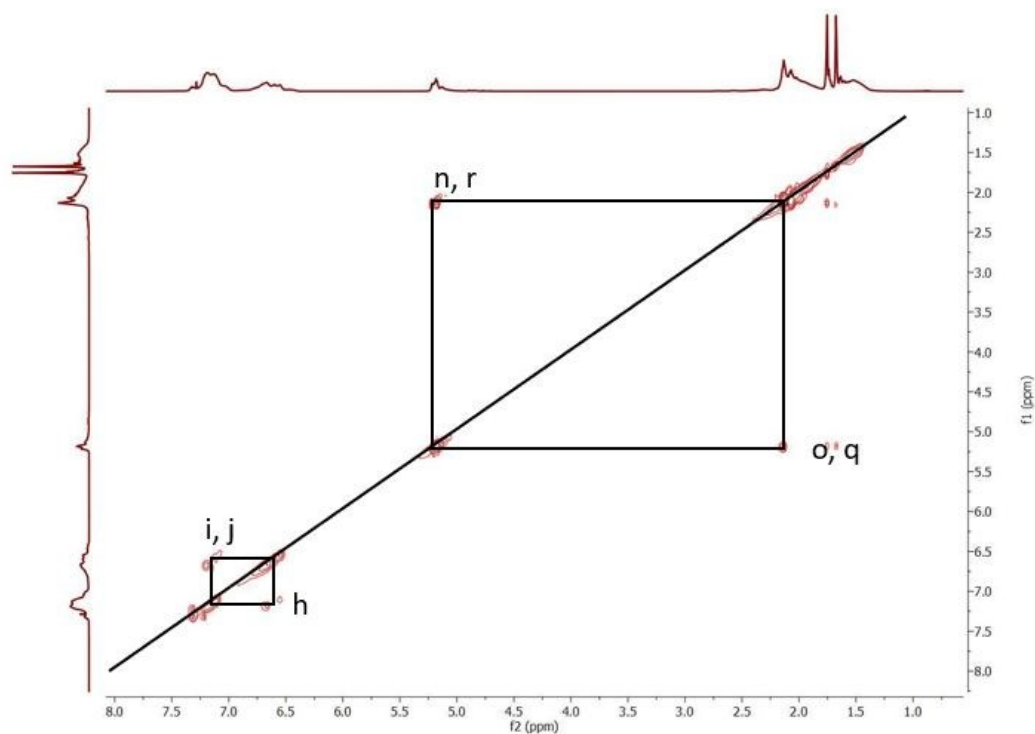


Figure S18: Assigned ^1H - and ^{13}C -NMR signals of $P(\text{Myr-co-S})$ synthesized in the presence of no modifier.

^1H : (CDCl_3 , 600 MHz, δ ppm): 7.36-6.84 (i, j); 6.84-6.31 (h); 5.19-4.98 (n,r); 4.94-4.59 (k'); 2.18-1.79 (k, o, p, q, n', p', f); 1.68 (t); 1.62 (u); 1.62-1.30 (e, o').

^{13}C : (CDCl_3 , 151 MHz, δ ppm): 151 (m'); 146-145 (g); 138 (m); 131 (s); 128-127 (h, j); 126-125 (j); 124 (r, n); 109 (k'); 45-40 (e, f); 37-27 (k, p, q, o, n', p'); 26-19 (o'); 25 (t); 18 (u)



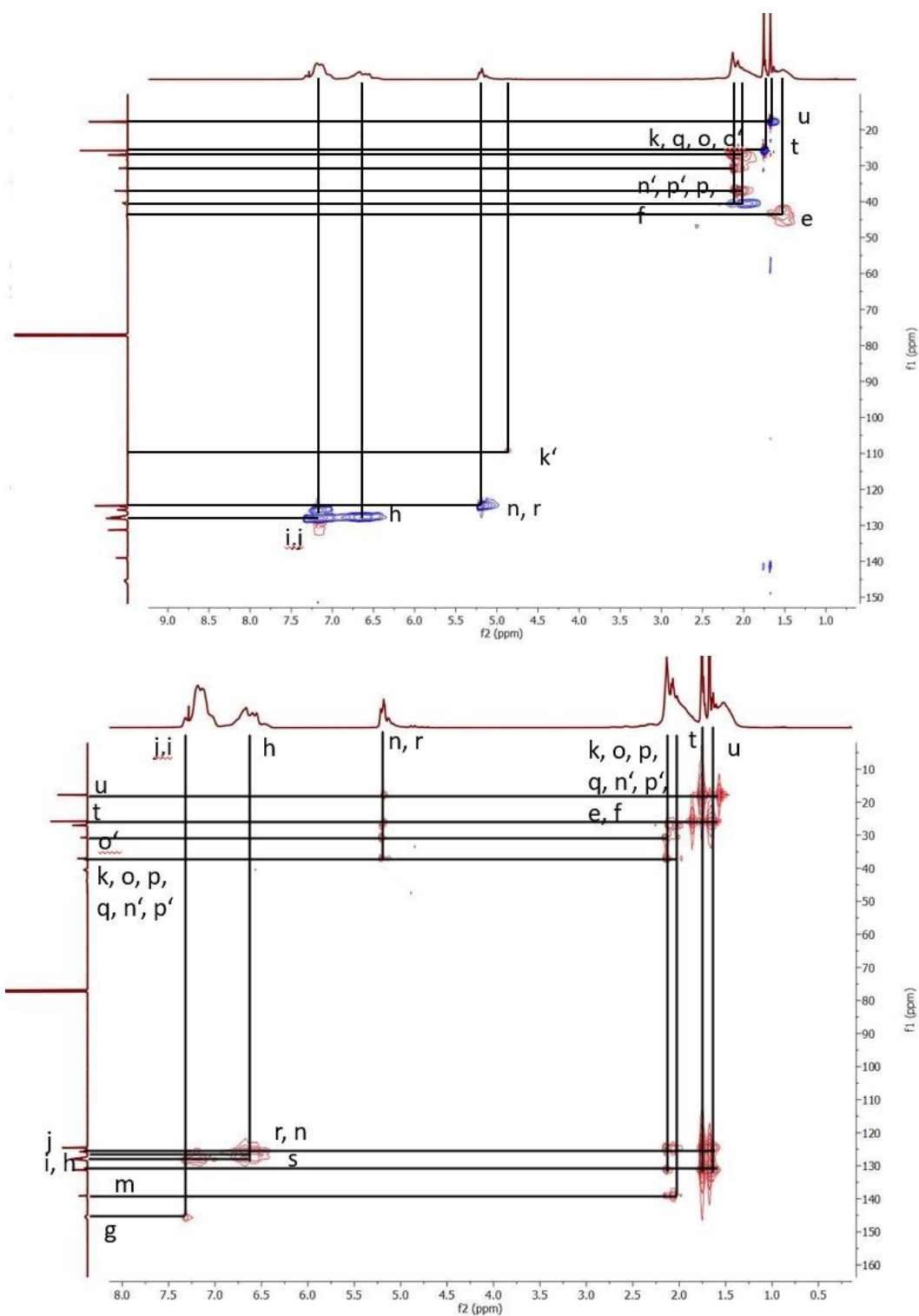


Figure S19: COSY, HSQC and HMBC spectra of P(Myrcos) synthesized in the presence of no modifier.

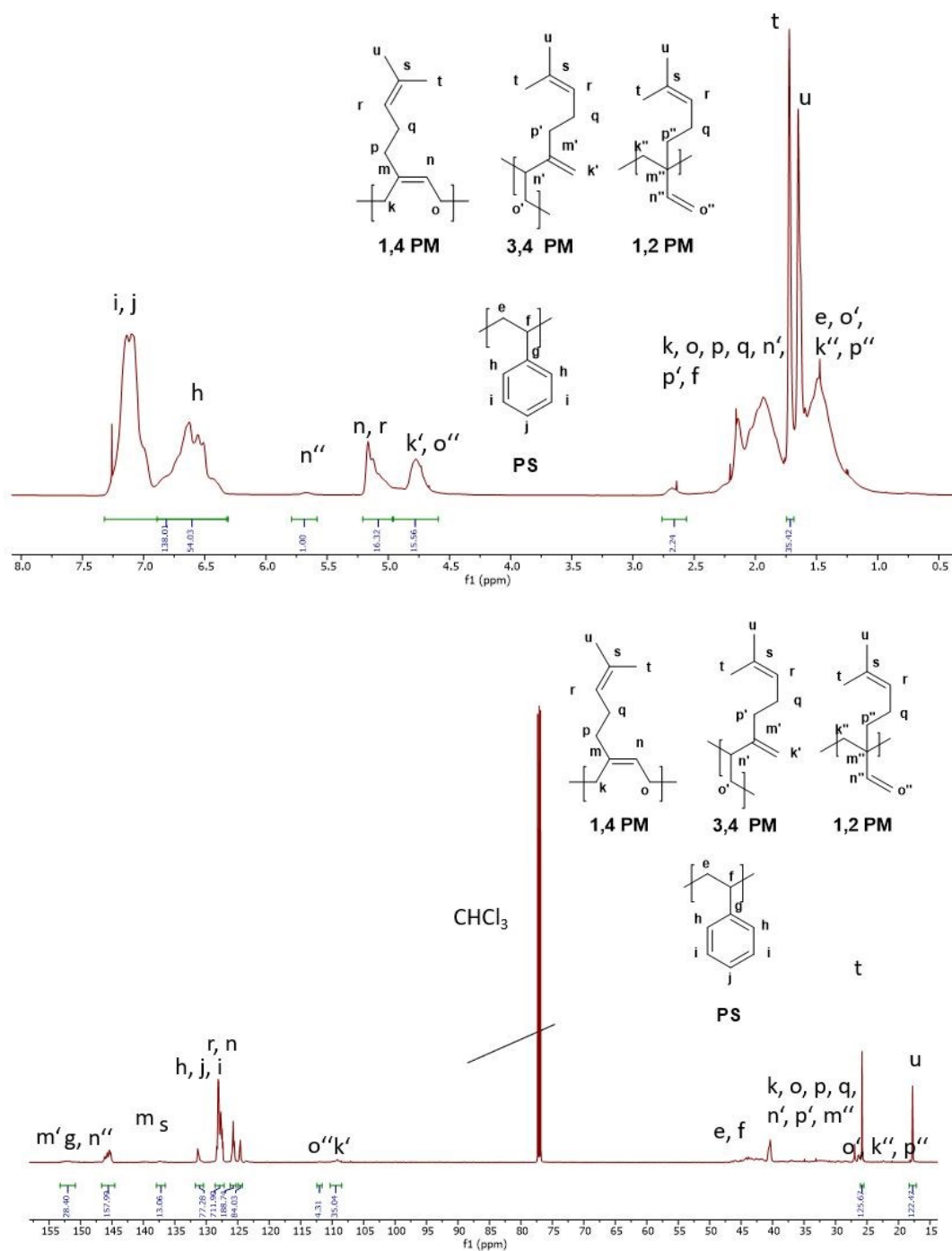
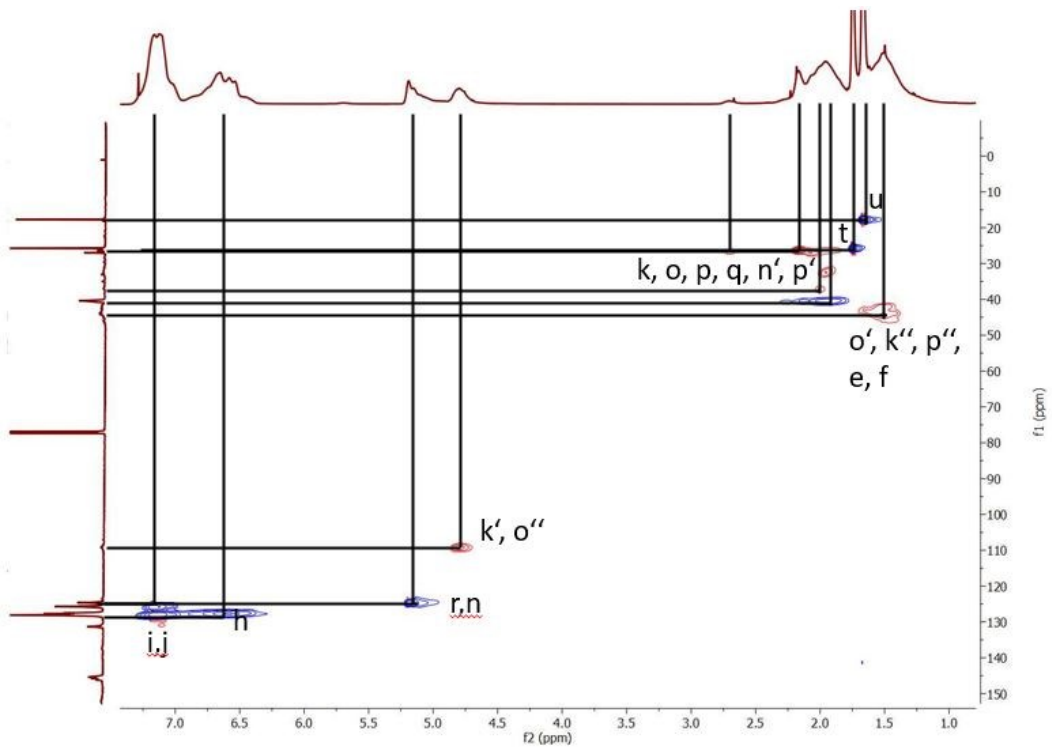
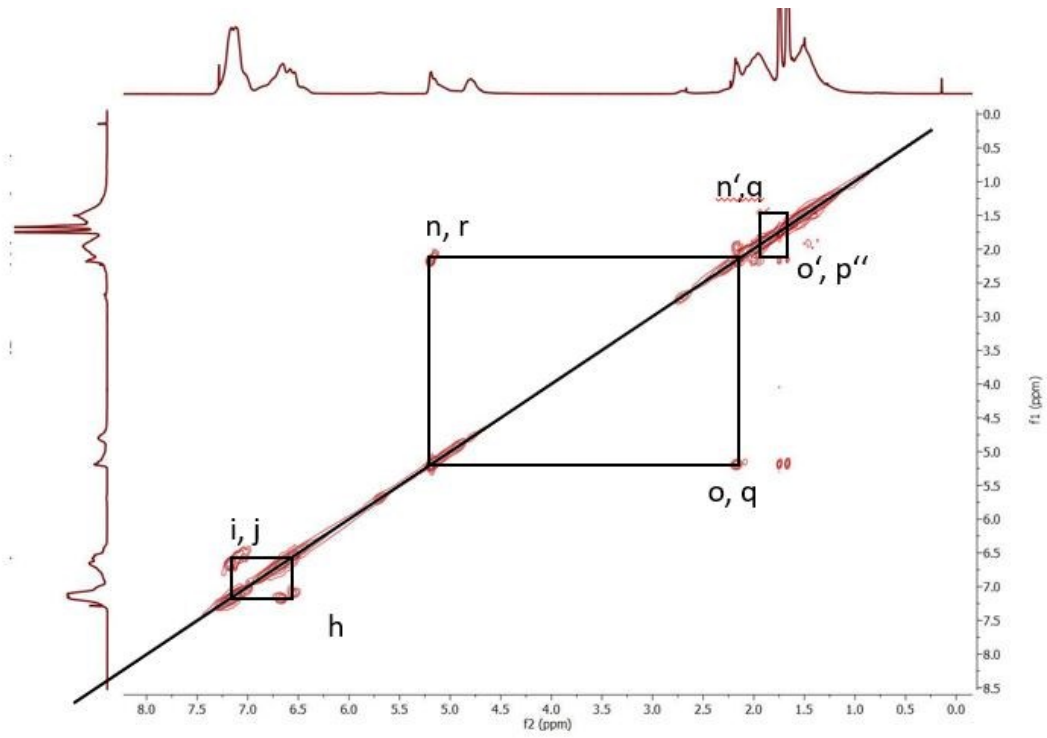


Figure S20: Assigned ^1H - and ^{13}C -NMR signals of $P(\text{Myr-co-S})$ synthesized in the presence of 2500 eq THF.

^1H : (CDCl_3 , 600 MHz, δ ppm): 7.36-6.84 (i, j); 6.84-6.31 (h); 5.82-5.60 (n''); 5.19-4.98 (n, r); 4.94-4.59 (k' , o''); 2.79-1.79 (k, o, p, q, n' , p' , f); 1.68 (t); 1.62 (u); 1.62-1.30 (e, p' , k'' , p'').

^{13}C : (CDCl_3 , 151 MHz, δ ppm): 151 (m'); 146-145 (g, n''); 138 (m); 131 (s); 128-127 (h, j); 126-125 (i); 124 (r, n); 112 (o''); 109 (k'); 45-40 (e, f); 37-27 (k, p, q, o, n' , p' , m''); 26-19 (o' , k'' , p''); 25 (t); 18 (u)



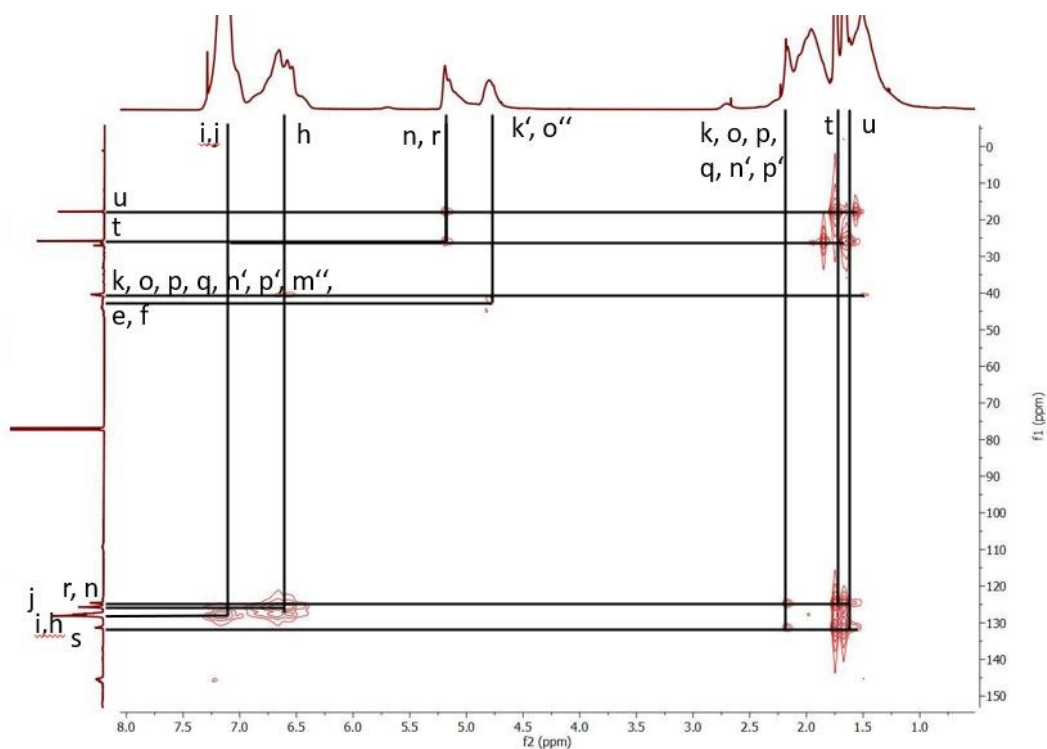


Figure S21: COSY, HSQC and HMBC spectra of *P(Myrcos)* synthesized in the presence of 2500 eq THF.

In the following Figures the modifier-dependent trend in microstructures is shown in the ^1H -NMR and $^{13}\text{C}_{\text{ig}}$ -NMR spectra. The increase in the intensities of the k' , o , and n signals in the ^1H -NMR spectra is clearly recognizable, as well as the decrease of the intensities of the n , r signals. Furthermore, the superposition of the i , j signal with the h signal with increasing modifier content of $0 \leq [\text{THF}]/[\text{Li}] \leq 8$ and $[\text{DTHFP}]/[\text{Li}] = 0.25$ is shown. This superposition decreases with further increasing modifier content again. In the $^{13}\text{C}_{\text{ig}}$ spectrum, the increase in the o and k' signals as well as the decrease of the r - and n -signals is shown.

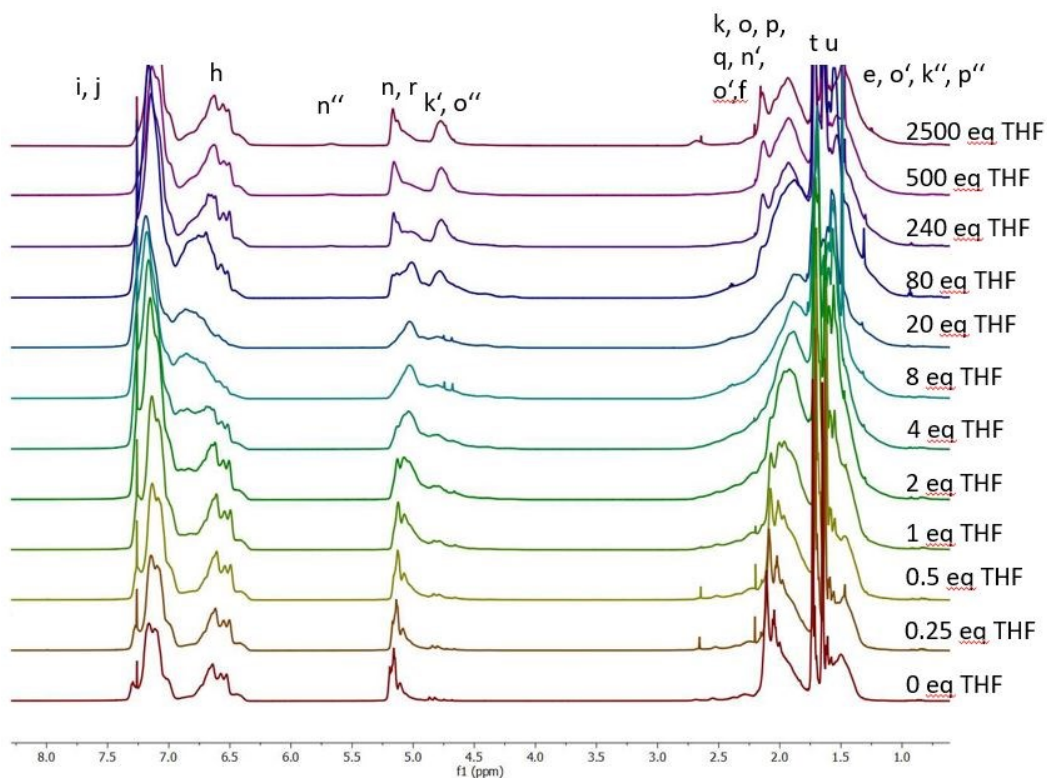


Figure S22: Plot of $^1\text{H-NMR}$ spectra (CDCl_3 , 600 MHz) of $P(\text{Myr-co-S})$ prepared in cyclohexane with $0 \leq [\text{THF}]/[\text{Li}] \leq 2500$.

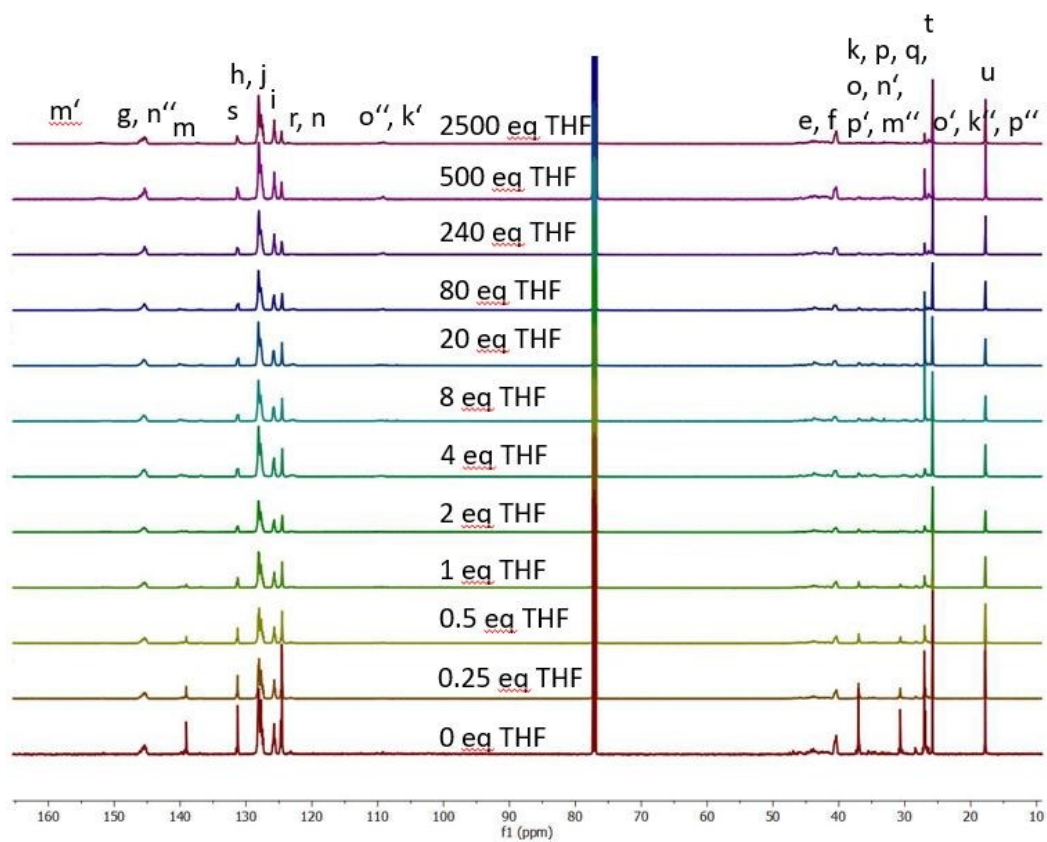


Figure S23: Plot of $^{13}\text{C}_g\text{-NMR}$ spectra (CDCl_3 , 151 MHz) of $P(\text{Myr-co-S})$ prepared in cyclohexane with $0 \leq [\text{THF}]/[\text{Li}] \leq 2500$.

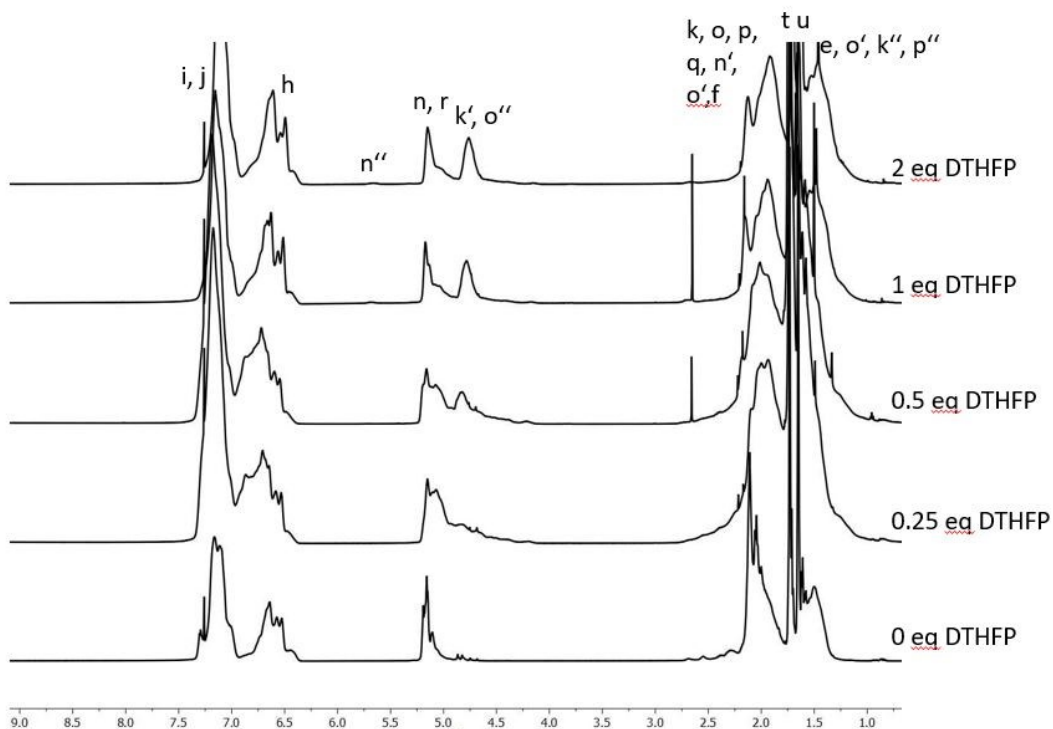


Figure S24: Plot of $^1\text{H-NMR}$ spectra (CDCl_3 , 600 MHz) of $P(\text{Myr-co-S})$ prepared in cyclohexane with $0 \leq [\text{DTHFP}]/[\text{Li}] \leq 2$.

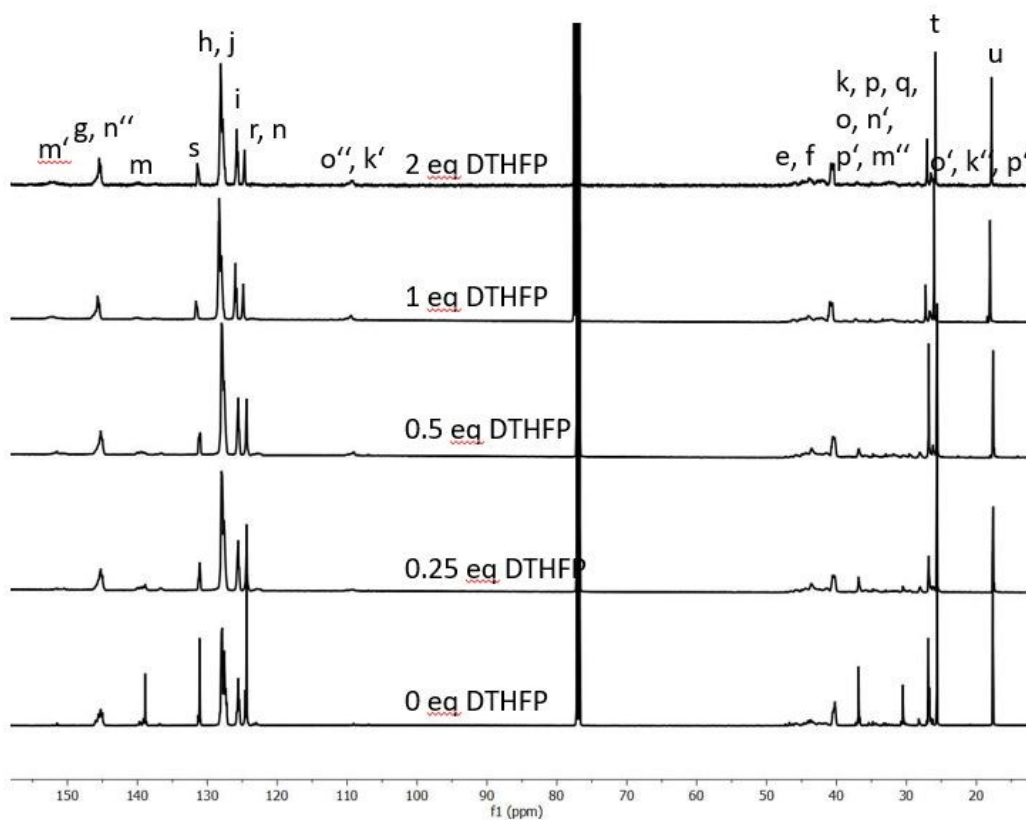


Figure S25: Plot of $^{13}\text{C}_{\text{ig-NMR}}$ spectra (CDCl_3 , 151 MHz) of $P(\text{Myr-co-S})$ prepared in cyclohexane with $0 \leq [\text{DTHFP}]/[\text{Li}] \leq 2$.

For the determination of the microstructure of polymyrcene in the copolymer P(Myrc-co-S) the interpretation of NMR spectroscopy was used.²⁴ More accurate values in comparison to the traditional mid-IR spectroscopy can be obtained by this method.²⁵ The assignments of the signals of the ¹H- and ¹³C-NMR spectra of the homopolymers were shown in the previous Figures. These are in agreement with the literature of polymyrcene²⁶ and polystyrene.^{21,22,27}

For the determination of the microstructure of polymyrcene, the method of M. Steube et al.¹⁶ cannot be applied due to the additional double bond in myrcene. Therefore, a new method based on the ¹H-NMR spectrum had to be developed. The isolated signal of n (5.82-5.60 ppm) is used. The integral of this signal reflects the content of 1,2-double bonds. The signals of k' and o'' (4.94-4.59 ppm) allow the determination of the 3,4 units. First the integral is divided by the number of hydrogen atoms present (here 2) and then the integral of n'' is subtracted thereof. The signals of n and r (5.19-4.98 ppm) are calculated for the determination of the 1,4-double bonds. From this integral, the integral of the signal n and the normalized integral of the signals k' and o are subtracted and then divided by two. Thus, a normalized integral is available for each microstructure. By applying the following equations we can calculate the proportion of microstructures present.

$$I_{1,2} = I(5.82 - 5.60\text{ppm})$$

$$I_{3,4} = \frac{I(4.94 - 4.59\text{ppm})}{2} - I_{1,2}$$

$$I_{1,4} = \frac{I(5.19 - 4.98\text{ppm}) - (I_{3,4} + I_{1,2})}{2}$$

$$C_{1,2} = \frac{I_{1,2}}{I_{1,2} + I_{3,4} + I_{1,4}}$$

$$C_{3,4} = \frac{I_{3,4}}{I_{1,2} + I_{3,4} + I_{1,4}}$$

$$C_{1,4} = \frac{I_{1,4}}{I_{1,2} + I_{3,4} + I_{1,4}}$$

Here $C_{1,2}$ stands for the fraction of 1,2-double bonds in the polymer and $I_{1,4}$ for the integral of the signal at 5.19-4.98 ppm after subtracting the remaining integrals. Since the signals used partially overlap, the determination of the integral limits is not unique but depends on the experimenter. Due to this, the determined proportions of the microstructure are subject to error and do not fully agree with the values known from the literature for block copolymers in pure THF.²⁸ The listed proportions are shown in Table 2 and Figure 4.

8 Thermal properties

The following Figures show the DSC curves of the copolymers obtained at 20 K/min; second heating cycle.

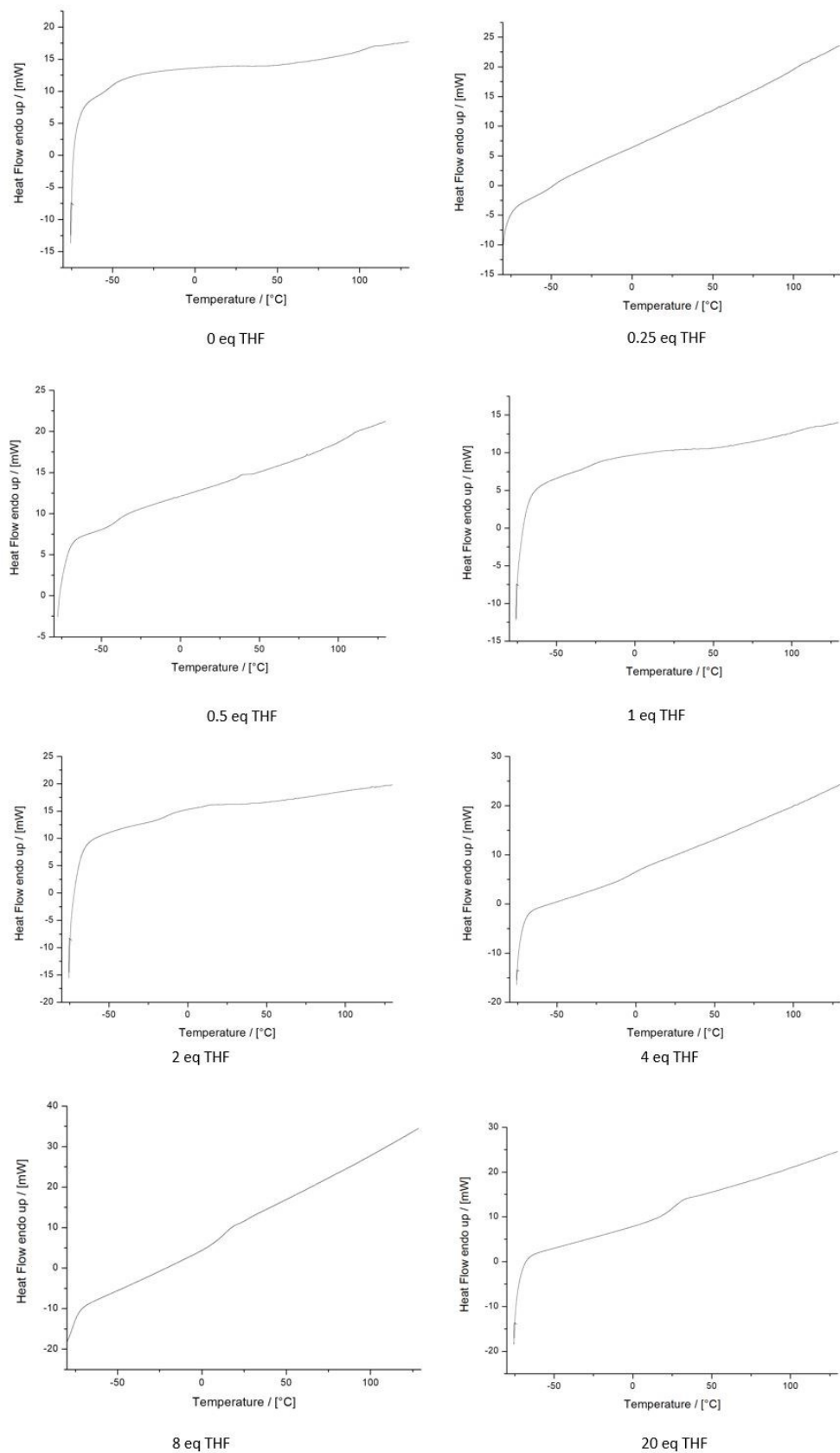


Figure S26a: DSC data of the P(My_r-co-S) synthesized at various [modifier]/[Li] ratios.

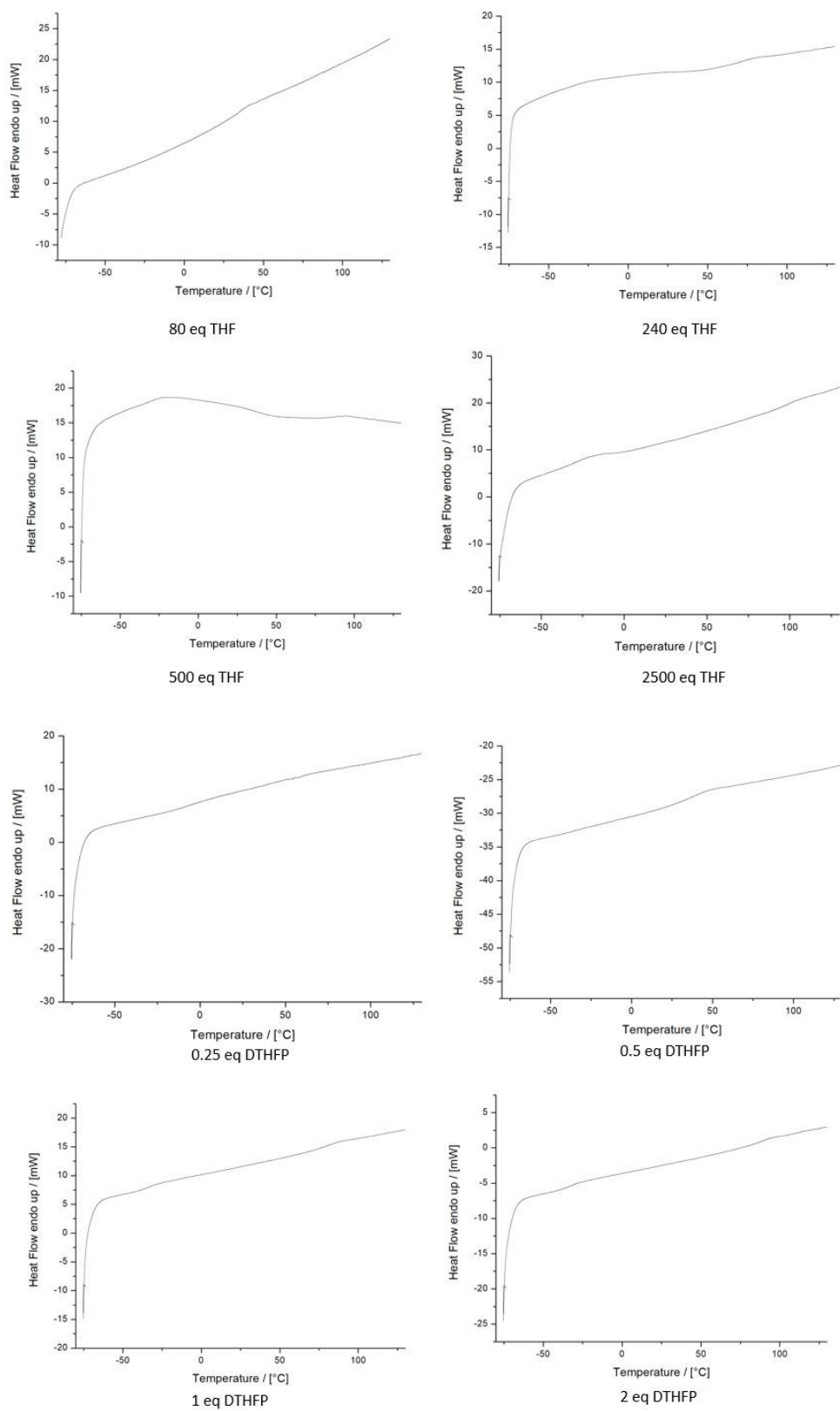


Figure S26b: DSC data of the P(Myrc-S) synthesized at various [modifier]/[Li] ratios.

9 Copolymer Morphologies

To increase the necessary contrast between the myrcene and styrene domains, the sample is stained with heavy metal salts. OsO_4 and RuO_4 are suitable for this procedure. OsO_4 reacts with the double bonds in the PMyr-rich domains and RuO_4 with double bonds of the PMyr-rich domains and the aromatic compounds of the PS-rich domains. In this way, the corresponding domains react with the heavy metal and to gain places with high electron density, which appear dark in the TEM image.^{16,29} OsO_4 is more suitable than RuO_4 for all samples, as can be seen in Figure S27. This can be due to the additional double bond in the myrcene backbone, since RuO_4 is associated with all the present double bonds and OsO_4 only reacts with those of the PM-rich phases.

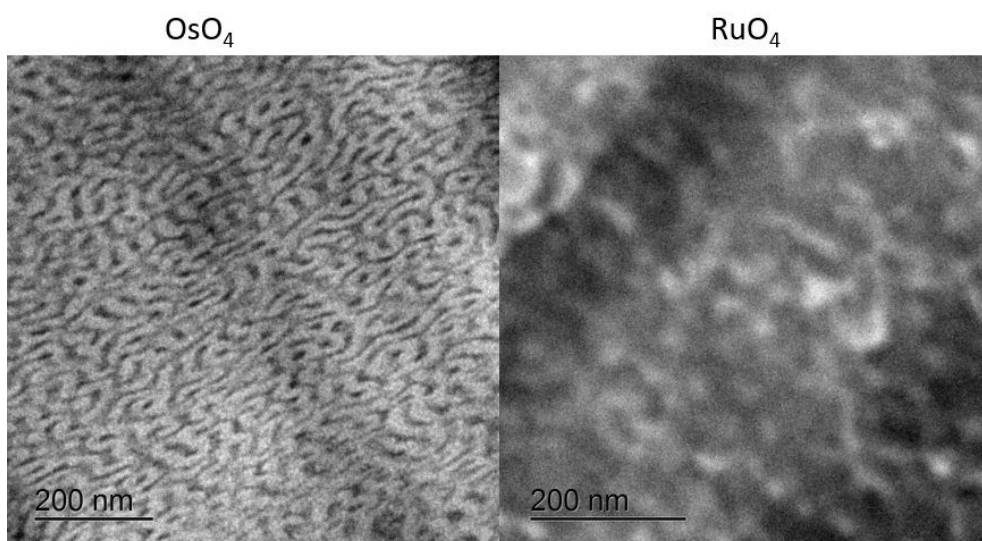


Figure S27: Comparison of the contrast of the copolymer P(Myrcene-co-Styrene) at the addition of $[\text{THF}]/[\text{Li}] = 240$ stained with OsO_4 and RuO_4 .

The determination of the volume of the PMyr- and PS-rich phase is hindered because of the gradient structure. For a block copolymer PS-*b*-PM with comparable properties to the synthesized gradient copolymers P(Myrcene-co-Styrene), would have a monomer feed of $f_{\text{Myr}} = 33.3 \text{ \% mol}$ and a volume fraction of $45\%_{\text{vol}}$. According to the theoretical phase diagram for diblock copolymers of Matsen and Bates *et al.* this should correspond to a lamellar structure.^{30,31} As already shown in other works, the gradient has an influence on the morphology that is formed.^{1,16} In this context, it influences not only the effective Flory-Huggins parameter, χ_{eff} , but also the effective volume fraction, ϕ , of the blocks. Not only the pure PMyr block, but also part of the gradient contributes to the observed PMyr-rich phase. To estimate the PS- and PMyr-rich volumes, the phase border has been redefined as the polymer volume at which random polymerization would occur.¹⁶ This corresponds to a volume fraction of 55 % styrene ($F_{\text{S,V}} = 0.55$) and is indicated below by a white line.

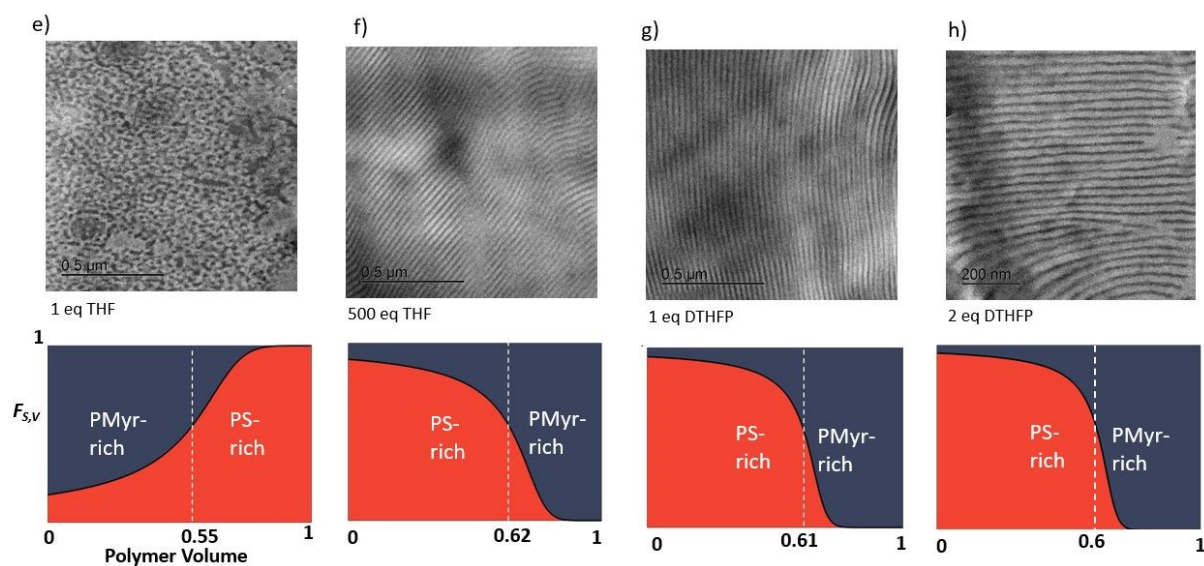


Figure S28: TEM images of P(S-co-Myr) synthesized at $[THF]/[Li] = 1, 500$ and $[DTHFP]/[Li] = 1, 2$ with their corresponding volume-based polymer compositions. The white line separates the PS-rich and PMyr-rich volumes. The contrast was enhanced using OsO_4 .

For $[THF]/[Li] = 1$ and 500 and $[DTHFP]/[Li] = 1$ and 2 lamellar morphologies are found. They have in comparison to the polymers with higher modifier amount ($[THF]/[Li] = 2500$ and $[DTHFP]/[Li] = 2$) the same lamellar morphology but more defects.

10 Mechanical properties

The determination of the Young's modulus, the toughness, the yield-point (ϵ_{yield} , σ_{yield}) and the break point (ϵ_{break} , σ_{break}) was carried out for each sample between three and twelve times, the respective mean values and standard deviations, calculated as associated error, are listed in Table S5. Exemplary results are shown in Fig. S29. Stress-strain curve were plotted for each [modifier]/[Li] ratio. The Young's modulus was determined by a linear fit for the range of small deformations, i.e., $\epsilon \leq 1.5\%$. The slope corresponds to the Young's modulus. At these low stresses, reversible stretching of the specimen occurs. The Young's modulus was determined only for samples exhibiting phase separation with a T_g above room temperature.¹⁶

The yield point (ϵ_{yield} and σ_{yield}) corresponds to the first maximum of the stress-strain curve. At the yield point the elastic behavior changes into plastic flow, indicating that the PS-domains start to disintegrate. Thus, it is only observed for samples that exhibit phase separation.³² Consequently, no yield point was determined for the copolymers P(Myrc-S) synthesized in the presence of [THF]/[Li] = 2, 4, 8, 20, 80 or [DTHFP]/[Li] = 0.25, 0.5. No yield point was observed for [THF]/[Li] = 240 either, which is related to the interconnected gyroid morphology in this case. Due to the three-dimensional structure, no yield point or plastic flow occurs. However, this structure significantly increased the Young's modulus.

The toughness was determined by direct numerical integration of the stress-strain curve using the Origin 7.5 software. The break point was chosen as the point, at which σ decreases sharply.

Table S5: Young's modulus, E, yield point, toughness and break point of P(Myrc-S) copolymers.

[THF]/[Li]	E [MPa]	ϵ_{yield} [%]	σ_{yield} [MPa]	Toughness [MPa]	ϵ_{break} [%]	σ_{break} [MPa]
0	219 ± 6	2.55 ± 0.04	5.0 ± 0.1	0.084 ± 0.005	2.55 ± 0.04	5.0 ± 0.1
0.25	140 ± 11	3.3 ± 0.4	3.5 ± 0.5	0.09 ± 0.02	3.7 ± 0.5	2.4 ± 0.4
0.5	154 ± 5	4.4 ± 0.1	4.57 ± 0.05	0.19 ± 0.01	5.39 ± 0.09	4.0 ± 0.2
1	158 ± 21	4.7 ± 0.6	4.6 ± 0.5	0.33 ± 0.06	9 ± 1	2.6 ± 0.3
2	-	-	-	2.8 ± 0.7	71 ± 21	2.3 ± 0.4
4	-	-	-	12 ± 1	933 ± 88	0.39 ± 0.09
8	-	-	-	11.6 ± 0.3	682 ± 14	2.87 ± 0.04
20	-	-	-	8 ± 2	756 ± 144	1.6 ± 0.5
80	-	-	-	17 ± 2	465 ± 31	4.1 ± 0.5
240	815 ± 25	-	-	0.58 ± 0.03	3.9 ± 0.2	23.8 ± 0.5
500	494 ± 81	3.8 ± 0.3	13 ± 2	0.50 ± 0.06	5.3 ± 0.8	8.2 ± 0.3
2500	288 ± 44	4.0 ± 0.3	7 ± 1	0.29 ± 0.04	5.3 ± 0.7	6 ± 1
[DTHFP]/[Li]						
0.25	-	-	-	19 ± 1	484 ± 31	3.89 ± 0.06
0.5	-	-	-	22.6 ± 0.6	326 ± 9	7.50 ± 0.05
1	397 ± 39	4.8 ± 0.1	12 ± 1	1.8 ± 0.6	17 ± 5	9.3 ± 0.6
2	319 ± 14	5.1 ± 0.7	8.9 ± 0.3	0.9 ± 0.2	11 ± 2	8.1 ± 0.1

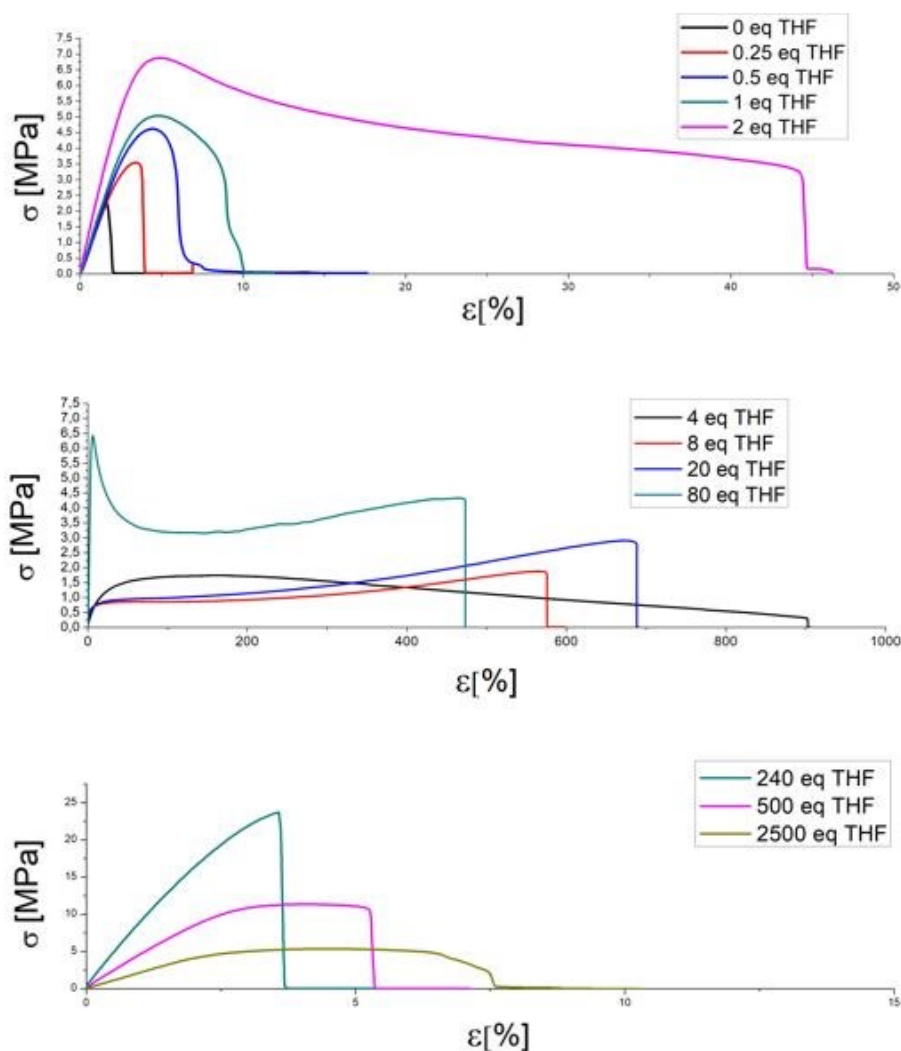


Figure S29: Representative stress-strain curves for the copolymer $P(\text{Myr-co-S})$ synthesized in the presence of different $[\text{modifier}]/[\text{Li}]$ ratios.

Since diblock type tapered structures are investigated that are incapable of forming a supramolecular network (like ABA triblock structures), no pronounced elastic behavior can be expected. This is confirmed by the observation that the yield point is already reached at very low strains. The molecular weight of approx. 80 kg/mol, is significantly higher than the entanglement molecular weight of both blocks (PS: 16.5 kg/mol and PMyr: 18 kg/mol).^{15,33} After an initial maximum σ , the tensile stress decreases again. In this flow region the specimen starts to constrict, and the cross section decreases. Although the apparent force decreases, relative to the actual cross section of the samples it increases.³⁴ This takes place until all existing chain loops are stretched and the complete specimen experiences the same strain. Only at this point the tensile stress increases again with increasing elongation.³⁵

For polymers synthesized in the presence of 0 to 4 eq THF the toughness and elasticity increase. With increasing modifier content from 4-80 eq THF highly plastic materials are obtained. Increasing the modifier content further from 240 to 2500 eq THF decreases the tensile force and increases the elasticity. The same trend is observed with DTHFP as modifier, albeit at much lower amounts, as discussed above.

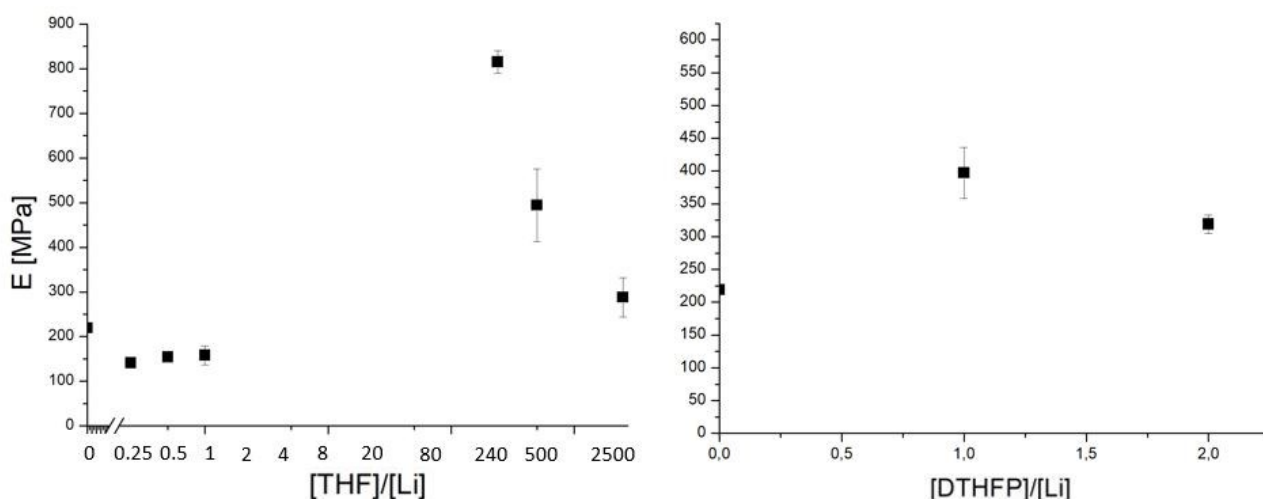


Figure S30: Young module as a function of the [modifier]/[Li] ratio.

Figure S30 shows the dependence of the Young's modulus on the [modifier]/[Li] ratio. An increase of the [THF]/[Li] ratio from 0 to 1 leads to a decrease of the Young's modulus, which is explained by the formation of a larger PMyr-rich phase.¹⁶ No Young's moduli could be determined for samples $2 \leq [\text{THF}]/[\text{Li}] \leq 80$ and $0.25 \leq [\text{DTHFP}]/[\text{Li}] \leq 0.5$, as they do not exhibit phase separation. Remarkably, the Young's modulus of the polymer for $[\text{THF}]/[\text{Li}] = 240$ is significantly higher than for all others due to its gyroid morphology discussed above.^{34,35} As the [modifier]/[Li] ratio further increases, the Young's modulus decreases again. This may be due to the inverted gradient or different lamellar thicknesses.³⁶ Clearly, the Young's moduli of copolymers synthesized in the presence of higher [modifier]/[Li] ratios are larger than those synthesized in pure cyclohexane, because the PS domains are not perturbed by myrcene units that lower the T_g .

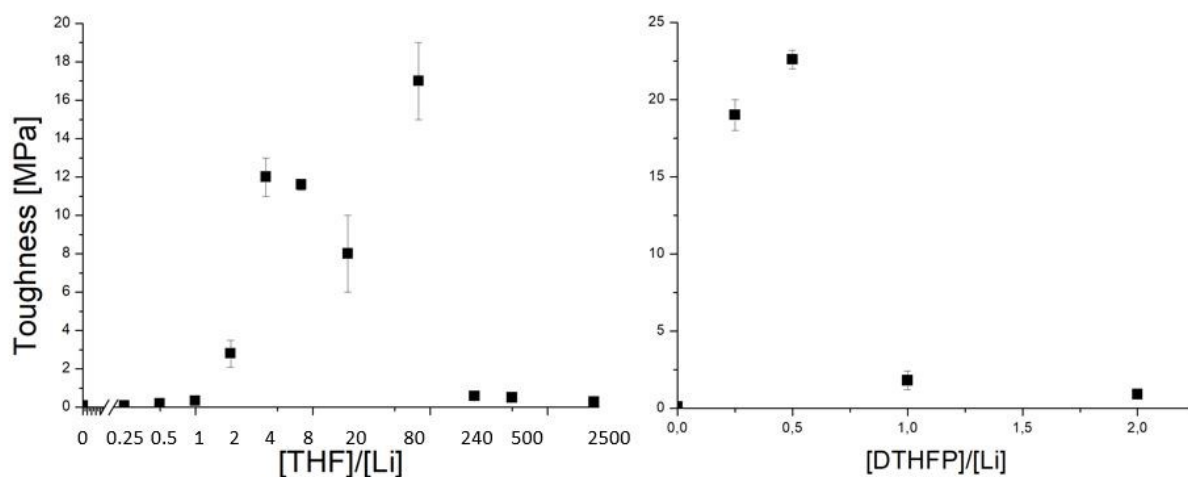


Figure S31: Toughness as a function of the [modifier]/[Li] ratio.

The toughness as a function of the [modifier]/[Li] ratio is shown in Figure S31. Very high values are obtained for polymers synthesized in the range $2 \leq [\text{THF}]/[\text{Li}] \leq 80$ and $0.25 \leq [\text{DTHFP}]/[\text{Li}] \leq 0.5$. This is due to viscoelastic flow, which shifts the break point to high elongations. The value for $[\text{THF}]/[\text{Li}] = 80$ deviates from the expected trend; this is probably due to the higher glass transition temperature of 34°C , which is slightly higher than the measurement temperature of 20°C , rendering the material harder.

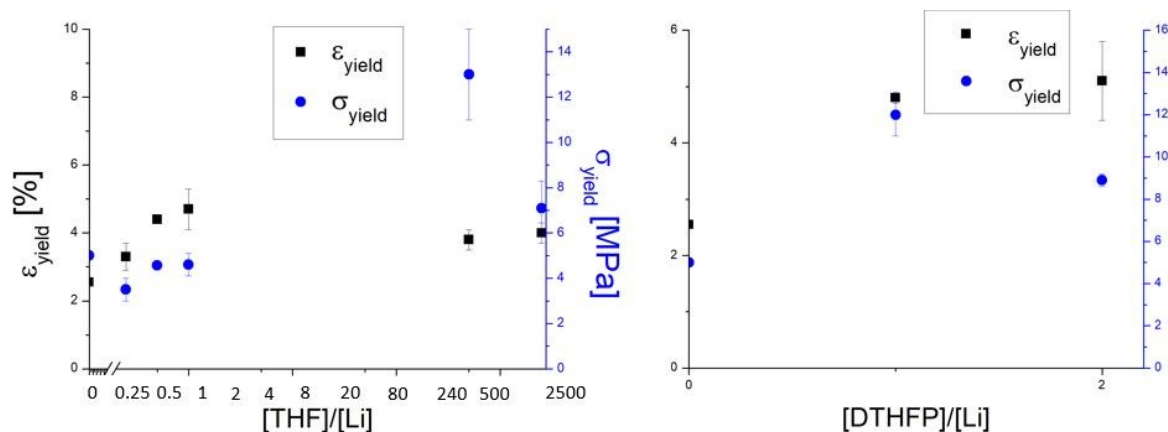


Figure S32: Yield point (ϵ_{yield} and σ_{yield}) as a function of the [modifier]/[Li] ratio.

The yield point (ϵ_{yield} , σ_{yield}) as a function of [modifier]/[Li] ratio is shown in Figure S32. No yield point was found in polymers synthesized at $2 \leq [\text{THF}]/[\text{Li}] \leq 80$ and $0.25 \leq [\text{DTHFP}]/[\text{Li}] \leq 0.5$. These polymers are in the disordered state and therefore do not show a transition from the elastic (stretching of the PMyr domains) to the plastic (rupture of the PS domains) region. Also, for $[\text{THF}]/[\text{Li}] = 240$ no yield point was found, due to the three-dimensional gyroid structure. ϵ_{yield} increases with increasing modifier ratio from $0 \leq [\text{THF}]/[\text{Li}] \leq 1$. This is explained by the different copolymer gradients. As a consequence, the volume of the PMyr domain increases, promoting elastic behavior. σ_{yield} increases to the same extent, only for $[\text{THF}]/[\text{Li}] = 0$ it is higher than expected.

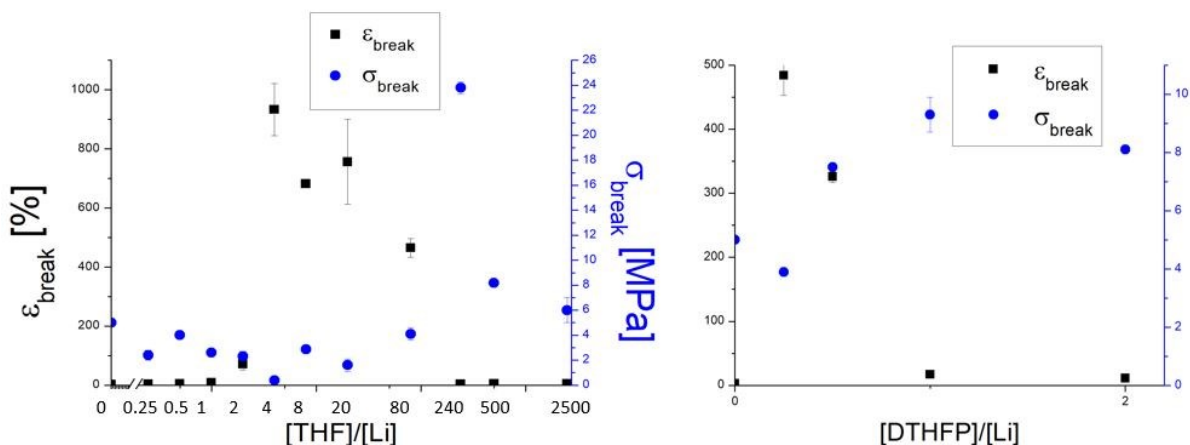


Figure S33: Break point (ϵ_{break} and σ_{break}) as a function of the [modifier]/[Li] ratio.

The break point (ϵ_{break} and σ_{break}) as a function of [modifier]/[Li] ratio is shown in Figure S33. ϵ_{break} increases for polymers synthesized between $0 \leq [\text{THF}]/[\text{Li}] \leq 4$ and $0 \leq [\text{DTHFP}]/[\text{Li}] \leq 0.25$ and then decreases again. Here, the strain between $4 \leq [\text{THF}]/[\text{Li}] \leq 80$ and $0.25 \leq [\text{DTHFP}]/[\text{Li}] \leq 0.5$ is significantly larger than for the remaining [modifier]/[Li] ratios. This further illustrates the disordered state of these samples, which allows for high plastic deformation. For $[\text{THF}]/[\text{Li}] = 4$ and $[\text{DTHFP}]/[\text{Li}] = 0.25$, the elongation is the largest because they have the lowest glass transition temperature in the disordered state. σ_{break} shows no clear trend, but is highest for $[\text{THF}]/[\text{Li}] = 240$, where the three-dimensional gyroid structure is present.^{34,37}

A comprehensive interpretation of these mechanical experiments proves to be difficult since various factors, such as morphology, glass transition temperature and microstructure, simultaneously exert an influence on the mechanical properties.

References:

- 1 M. Steube, T. Johann, M. Plank, S. Tjaberings, A. H. Gröschel, M. Gallei, H. Frey and A. H. E. Müller, *Macromolecules*, 2019, **52**, 9299–9310.
- 2 M. Steube, T. Johann, H. Hübner, M. Koch, T. Dinh, M. Gallei, G. Floudas, H. Frey and A. H. E. Müller, *Macromolecules*, 2020, **53**, 5512–5527.
- 3 A. Jouyban, S. Soltanpour and H. K. Chan, *Int. J. Pharm.*, 2004, **269**, 353–360.
- 4 F. E. Critchfield, J. A. Gibson and J. L. Hall, *J. Am. Chem. Soc.*, 1953, **75**, 6044–6045.
- 5 G. E. Papanastasiou and I. I. Ziogas, *J. Chem. Eng. Data*, 1991, **36**, 46–51.
- 6 V. Jaacks, *Die Makromol. Chemie*, 1972, **161**, 161–172.
- 7 V. Jaacks, *Angew. Chemie*, 1967, **79**, 419–419.
- 8 V. E. Meyer and G. G. Lowry, *J. Polym. Sci. Part A Gen. Pap.*, 1965, **3**, 2843–2851.
- 9 F. T. Wall, *J. Am. Chem. Soc.*, 1941, **63**, 1862–1866.
- 10 J. Blankenburg, E. Kersten, K. Maciol, M. Wagner, S. Zorbakhsh and H. Frey, *Polym. Chem.*, 2019, **10**, 2863–2871.
- 11 B. S. Beckingham, G. E. Sanoja and N. A. Lynd, *Macromolecules*, 2015, **48**, 6922–6930.
- 12 N. A. Lynd, R. C. Ferrier and B. S. Beckingham, *Macromolecules*, 2019, **52**, 2277–2285.
- 13 A. Dev, A. Rösler and H. Schlaad, *Polym. Chem.*, 2021, **12**, 3084–3087.
- 14 M. Steube, T. Johann, M. Plank, S. Tjaberings, A. H. Gröschel, M. Gallei, H. Frey and A. H. E. Müller, *Macromolecules*, 2019, **52**, 9299–9310.
- 15 C. Wahlen, J. Blankenburg, P. von Tiedemann, J. Ewald, P. Sajkiewicz, A. H. E. Müller, G. Floudas and H. Frey, *Macromolecules*, 2020, **53**, 10397–10408.
- 16 M. Steube, T. Johann, H. Hübner, M. Koch, T. Dinh, M. Gallei, G. Floudas, H. Frey and A. H. E. Müller, *Macromolecules*, 2020, **53**, 5512–5527.
- 17 M. Morton and L. J. Fetters, *J. Polym. Sci. Part A Gen. Pap.*, 1964, **2**, 3311–3326.
- 18 S. Bywater and D. J. Worsfold, *Can. J. Chem.*, 1962, **40**, 1564–1570.
- 19 M. Steube, T. Johann, E. Galanos, M. Appold, C. Rüttiger, M. Mezger, M. Gallei, A. H. E. Müller, G. Floudas and H. Frey, *Macromolecules*, 2018, **51**, 10246–10258.
- 20 L. J. Fetters, D. J. Lohse, D. Richter, T. A. Witten and A. Zirkel, *Macromolecules*, 1994, **27**, 4639–4647.
- 21 F. A. Bovey, G. V. D. Tiers and G. Filipovich, *J. Polym. Sci.*, 1959, **38**, 73–90.
- 22 V. D. Mochel, *Macromolecules*, 1969, **2**, 537–540.
- 23 D. L. Handlin, US 6,699,941 B1 to Kraton Polymers U.S. LLC, 2004.
- 24 H. Y. Chen, *Anal. Chem.*, 1962, **34**, 1134–1136.
- 25 D. J. Worsfold and S. Bywater, *Rubber Chem. Technol.*, 1965, **38**, 627–635.
- 26 P. Sarkar and A. K. Bhowmick, *RSC Adv.*, 2014, **4**, 61343–61354.
- 27 H. J. Harwood, T. K. Chen and F. T. Lin, *ACS Symp. Ser.*
- 28 J. Bareuther, M. Plank, B. Kuttich, T. Kraus, H. Frey and M. Gallei, *Macromol. Rapid Commun.*, 2020, **2000513**, 1–9.
- 29 H. Schmalz, A. Böker, R. Lange, G. Krausch and V. Abetz, *Macromolecules*, 2001, **34**, 8720–8729.
- 30 A. K. Khandpur, S. Förster, F. S. Bates, I. W. Hamley, A. J. Ryan, W. Bras, K. Almdal and K. Mortensen, *Macromolecules*, 1995, **28**, 8796–8806.
- 31 M. W. Matsen and F. S. Bates, *Macromolecules*, 1996, **29**, 1091–1098.
- 32 D. Long and P. Sotta, *Rheol. Acta*, 2007, **46**, 1029–1044.
- 33 J. E. Mark, *Physical Properties of Polymers Handbook*, Springer New York, New York, NY, 2007.

- 34 B. J. Dair, C. C. Honeker, D. B. Alward, A. Avgeropoulos, N. Hadjichristidis, L. J. Fetters, M. Capel and E. L. Thomas, *Macromolecules*, 1999, **32**, 8145–8152.
- 35 S. Spiegelberg, *Characterization of Physical, Chemical, and Mechanical Properties of UHMWPE*, Elsevier Inc., Oxford, 2nd Ed., 2009.
- 36 S. Luo, D. T. Grubb and A. N. Netravali, *Polymer (Guildf.)*, 2002, **43**, 4159–4166.
- 37 D. J. Kinning, E. L. Thomas, D. B. Alward, L. J. Fetters and D. L. Handlin, *Macromolecules*, 1986, **19**, 1288–1290.